JOURNAL OF GEOPHYSICAL RESEARCH, VOL. 114, A01304, doi:10.1029/2008JA013683, 2009

Distinctive plasma density features of the topside ionosphere and their electrodynamics investigated during southern winter

Ildiko Horvath[1] and Brian C. Lovell[1,2]

Received 15 August 2008; revised 2 November 2008; accepted 20 November 2008; published 16 January 2009.

[1] This study utilizes a novel technique to map the Defense Meteorological Satellite Program (DMSP) data across the two hemispheres to learn about the morphology and plasma composition of the topside ionosphere, and the underlying ionospheric dynamics. In the southern winter hemisphere, the regional maps tracked a heavy-ion (Ni-O^+) trough, aurora zone, polar hole, and large plasma density depletion. The latter appeared in the region of the South Atlantic Magnetic Anomaly (SAMA). The electron temperature (Te) map detected the thermal characteristics of these features, while the plasma drifts and flux maps tracked their dynamics. Results show that there were special electrodynamic effects in the SAMA region due to the low magnetic field and high conductivity. These increased the vertical downward (V_Z) and the westward (V_Y) drifts. Independently, the V_Z and V_Y maps registered the affected area that was depleted in heavy ions and rich in light ions. Some field-aligned profiles tracked the impact of these SAMA effects on the heavy-ion trough, which was a stagnation trough and appeared markedly differently at different longitudes. At trough latitudes ((56 ± 4)°S (geomagnetic) when Dst_{av} = 0 nT), the elevated electron temperatures forming a Te peak indicated subauroral heating effects. A statistical study modeled the magnetic activity dependence of the Te peak's magnitude and location and revealed their linear correlation with the activity level. Statistically, the Te peak increased [10.226 ± 1.355]°K and moved equatorward [0.051 ± 0.009]° (geomagnetic) per 1 nT decrease in the averaged Dst index. Per 1 nT increase in the averaged AE index, its magnitude increased [1.315 ± 0.444]°K and the equatorward movement was [0.014 ± 0.003]°.

Citation: Horvath, I., and B. C. Lovell (2009), Distinctive plasma density features of the topside ionosphere and their electrodynamics investigated during southern winter, *J. Geophys. Res.*, *114*, A01304, doi:10.1029/2008JA013683.

1. Introduction

[2] In the equatorial and low midlatitude ionospheric regions, the distribution of plasma is controlled by the coupled processes of plasma diffusion, **E** × **B** drifts, thermospheric neutral winds and chemical processes. The daytime (nighttime) *F* region plasma is transported by a vertical upward (downward) **E** × **B** drift, created by the interaction of ionospheric **E** field and geomagnetic **B** field, over the dip equator, and by field-aligned diffusions on both sides of the dip equator [*Hanson and Moffett*, 1966; *Balan and Bailey*, 1995; *Balan et al.*, 1997; *Bailey et al.*, 1997]. These processes have a tendency to create a plasma distribution symmetric to the dip equator. However, this tendency is interrupted by the meridional and transequatorial neutral winds, which move the plasma along the magnetic field lines and produce hemispheric and interhemispheric plasma flows, respectively, and by the accompanying chemical processes [*Titheridge*, 1995; *Kil et al.*, 2006]. Significant longitudinal variations in plasma distribution reflect the corresponding variations of the underlying mechanisms. Major causes of such variations are related to the longitudinal variations in the **B** field intensity and declination. Field-aligned hemispheric and interhemispheric plasma flows maximize in regions where the meridional and zonal winds have similar components. Their combination maximizes during southern winter in the 300°E–340°E (geographic) longitude sector, over the Atlantic. There, the declination (D) is westerly and high (21°) and the field-aligned interhemispheric plasma flows are directed from the northern summer to the southern winter hemisphere [*Venkatraman and Heelis*, 2000]. However, over the South Atlantic, the total **B** field intensity is anomalously low (~22.8 • 10^3 nT [*Trivedi et al.*, 2005]), a phenomenon known as the South Atlantic Magnetic Anomaly (SAMA), that makes the **E** × **B** drift unusually strong, since its magnitude is **E** × **B**/B^2 [*Kendall and Pickering*, 1967]. Furthermore, there are special electrodynamic effects in the SAMA region that can further increase the magnitude of the **E** × **B** drift by increasing the **E** field. Because of these electrodynamics, the plasma density is highly variable over the South Atlantic and can be anomalously low [*Abdu et al.*, 2005]. Produced by quiet time E layer energetic particle precipitations [*Abdu and*

[1]SAS, School of Information Technology and Electrical Engineering, University of Queensland, Brisbane, Queensland, Australia.
[2]National Information and Communications Technology Australia, University of Queensland, Brisbane, Queensland, Australia.

0148-0227/09/2008JA013683

Batista, 1977], there is an enhanced E layer ionization over the South Atlantic. The E layer conductivity is a maximum, where the magnetic field is a minimum, at the center of the SAMA (310°E, 10°S; geographic), over south Brazil, and decreases with increasing distance away from that center, toward the African continent. This can result in a westward conductivity gradient over the South Atlantic (indicated as $\Delta\Sigma$ [*Abdu et al.*, 2003]) that can add to the background conductivity gradient, which is also westward directed during the post-sunset hours, and thus can create a locally high (or modified) conductivity distribution that is a regular feature of the ionosphere over the SAMA [*Abdu et al.*, 2005]. According to the model simulations of *Abdu et al.* [2005], this increased conductivity will create a significantly stronger vertical $\mathbf{E} \times \mathbf{B}$ at the prereversal enhancement over Brazil (east coast of South America) than over Jicamarca (west coast of South America).

[3] In the high-latitude ionosphere, the plasma distribution is dominated by horizontal $\mathbf{E} \times \mathbf{B}$ convection that moves the plasma across the magnetic field lines. This plasma convection is triggered by the interaction of the cross-polar **E** field and geomagnetic **B** field, and directs the plasma motion in a pattern that is dependent on the interplanetary magnetic field's (IMF) orientation [*Heelis*, 1984]. The superposition of convection and co-rotation **E** fields gives rise to flow stagnation, that is, the plasma becomes trapped between the regions of eastward co-rotating plasma flow and westward convection flow [*Whalen*, 1989]. First suggested by *Knudsen* [1974], plasma stagnations occurring in darkness produce electron density depletions larger than expected and are the main driving mechanisms forming a midlatitude trough that is also called main trough. The trough manifests itself as a plasma density depletion relative to the ionosphere around it. In both hemispheres, on the equatorward edge of the auroral zone, the trough has a mean position at ~65° (geomagnetic; corresponding to $L \approx 4$ [*Brinton et al.*, 1978; *Moffett and Quegan*, 1983; *Rodger et al.*, 1992]). There, the electron temperature (Te) becomes elevated. Called subauroral Te enhancement, this is a quasi-permanent feature on the night-side in the altitude range of 350 km–1000 km [*Kozyra et al.*, 1986; *Fok et al.*, 1991; *Prolss*, 2006, 2007]. When slow plasma drifts take place in the absence of solar radiation, they produce electron density depletions larger than expected. First suggested by *Brinton et al.* [1978], a polar hole is formed by flux tubes circulating in the permanent darkness and its minimum Te indicates the absence of heat sources. In the slow convection region of the polar cap, the polar hole develops in the form of a marked electron density depletion [*Crowley et al.*, 1993, and references therein]. There, the electron density is able to decay to low values before the plasma flux tubes enter regions of strong ionization [*Sojka et al.*, 1991].

[4] Since the trough was first detected in the northern hemisphere by *Muldrew* [1965] and *Sharp* [1966], it has been the subject of experimental and theoretical studies that are comprehensively reviewed by *Moffett and Quegan* [1983] and *Rodger et al.* [1992]. Although the recent trough studies, utilizing complex data sets such as ISS-b [*Karpachev*, 2003], DE-2 [*Prolss*, 2006, 2007] and various analysis techniques such as ionospheric tomography [*Aladjev et al.*, 2001; *Yizengaw and Moldwin*, 2005; *Yizengaw et al.*, 2005; *Voiculescu et al.*, 2006], increase significantly our understanding, the current knowledge of the trough phenomenology is still incomplete. Furthermore, studies, investigating the southern trough with other prominent plasma density features or in the vicinity of the SAMA, where the plasma density is highly variable, and the plasma environment of these features, are still non existent. This study, for the first time, aims to carry out such a complex investigation. It has two major aims. One is to investigate these prominent plasma density features and their plasma environment, plus the electrodynamic processes of the SAMA and their effects on both the midlatitude ionosphere and the southern nighttime main trough during the 2000 southern winter. Another main aim of this work is to carry out a statistical study on both the southern nighttime winter trough and the subauroral Te peak in order to find out their average locations and how they correlate with the various averaged geomagnetic indices. To succeed, this study utilizes simultaneous plasma measurements collected by the F13 spacecraft of the Defense Meteorological Satellite Program (DMSP), a novel mapping technique to track these features and the various geophysical factors of their plasma environment in the topside ionosphere, the modeled magnetic field lines to find out the alignment of the DMSP passes, and a statistical analysis for modeling. A series of latitudinal profiles, some are field-aligned and some are oriented at midlatitudes and at high latitudes perpendicular to the magnetic field lines, provide some interesting observations.

2. Database, Instrumentation, and Methodology

[5] A database, provided by 528 satellite passes during the months of 2000 southern winter (June–August inclusive) was created. It contains a set of in situ measurements of the Flight 13 (F13) spacecraft that is one of the current DMSP series. Each spacecraft is three-axis stabilized, and carries a SSJ/4 detector and a SSIES detector [*Hairston et al.*, 1997]. SSJ4 is a term for Special Sensor Precipitating Electron and Ion Spectrometer, and SSIES stands for Special Sensors-Ions, Electrons and Scintillation. Computed from the one-second resolution measurements made with the SSJ/4 detector, DMSP spectrograms are readily available to the science community. This study utilizes a small collection of F13 spectrograms and the numerical data of the 528 satellite passes from the SSIES thermal plasma analysis package. The quality of numerical data is rated by flags. In this study, measurements flagged as "good" and "caution" were utilized only. This database contains the measurements of ion concentration (Ni in i^+/cm^3), electron temperature (Te in °K), fractional amounts of O^+, He^+ and H^+ (indicated as $[O^+]$, $[He^+]$ and $[H^+]$) and cross-track plasma drift components (V_Y and V_Z; in m/s). Computed as the product of plasma drift and Ni, the horizontal (F_Y) and vertical (F_Z) cross-track plasma flux components (in $[i^+/(cm^2 \bullet s)]$) were added to this database. Like the other DMSP spacecraft, the F13 circles the Earth in the 850–870 km altitude range in a 96°-inclined Sun-synchronous orbit with an orbital period of 101 min. The F13 spacecraft completes around 14 orbits each day. Each orbit is made up of an ascending (northbound) pass and a descending (southbound) pass. The same passes of two consecutive orbits are separated by ~25° (lat.; see Figure 1a and more details from *Horvath* [2007]). For this study, the southbound passes were suitable, as they covered the local nighttime hours at southern midlatitudes and high latitudes. At ~55°S

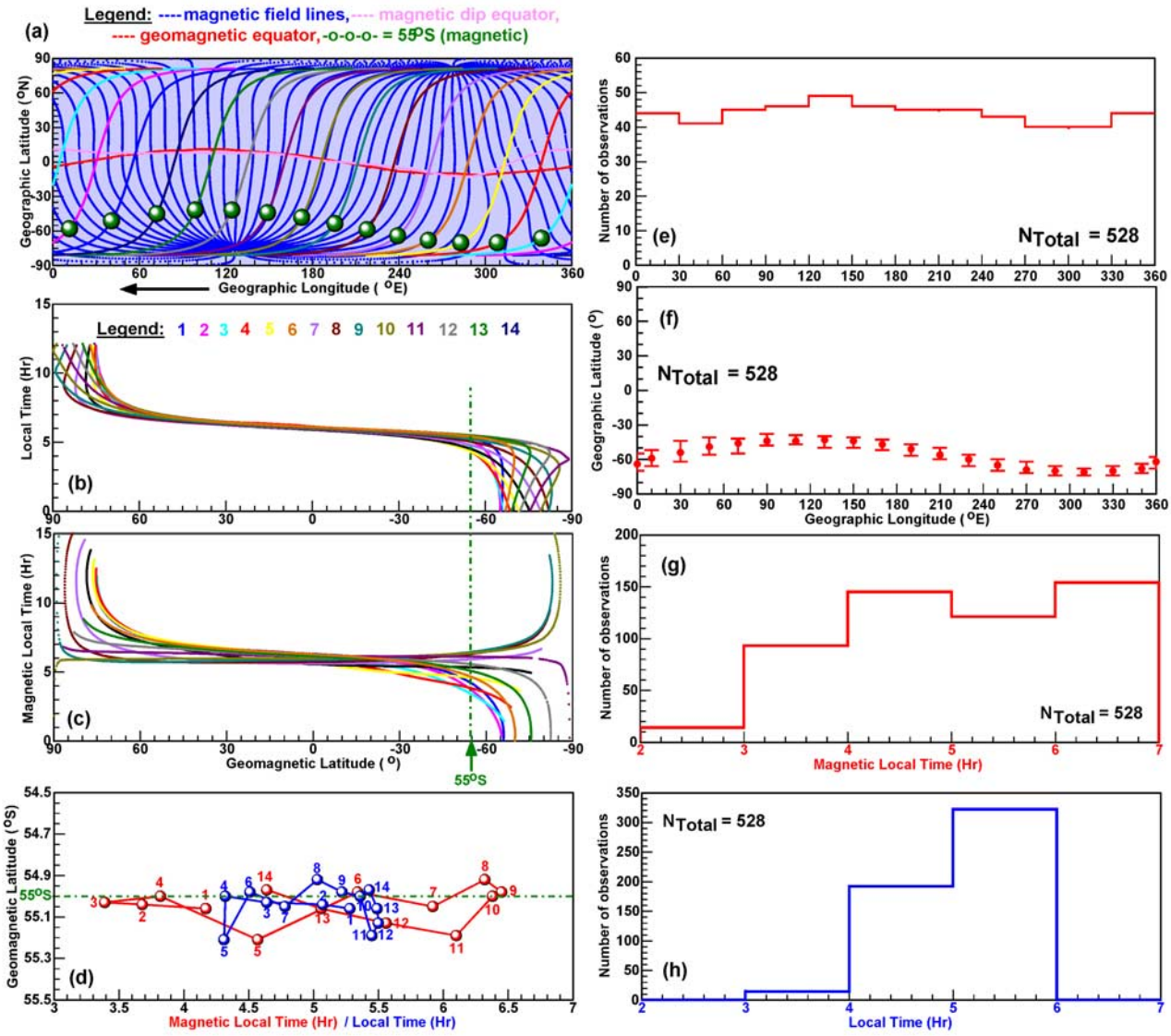

Figure 1. (a) The global magnetic field-line map shows all the 14 southbound passes completed by the F13 spacecraft on 2 August 2000 and the trough positions tracked at ~55°S (geomagnetic). These passes' (b) MLT and (c) LT are plotted in geomagnetic latitude. (d) At trough latitude (~55°S), the MLT (indicated in red) and LT (indicated in blue) varied differently. (e) The longitudinal distribution of the 528 detections and (f) their geographic location, plus their (g) magnetic local time and (h) local time distributions, are also shown.

(geomagnetic), the trough was tracked (see Figure 1a). In Table 1, the average variation of local time (LT; in decimal hours), magnetic local time (MLT; in decimal hours) and geographic latitude is compiled for the Australian and American longitude sectors. The data from these F13 passes provided observations in a varying LT and MLT frame. As Figure 1b shows, the LT varied from midday (~90°N; geomagnetic), through 6 LT (at the equator), to midnight (at ~81°S). However, the MLT exhibited a greater variation over geomagnetic latitudes higher than ±30° (see Figure 1c). There was only a 2-h LT variation between 50°N and 45°S from 7 LT to 5 LT (see Table 1). At trough latitudes (~55°S; geomagnetic), the LT varied between 4.3 Hr and 5.5 Hr, while the MLT changed between 3.4 Hr and 6.7 Hr (see Figure 1d). Altogether 528 trough observations were registered. Their longitudinal distribution is shown by a histogram in Figure 1e. From these observations, an average trough position with a minimum and a maximum position (indicated by the error bars) was also computed for each 20° (lon; geographic) degree (see Figure 1f). Two histograms illustrate the LT (see Figure 1g) and the MLT (see Figure 1h) distribution of the trough detections.

[6] In order to describe the state of the topside ionosphere, the observational data provided by these 528 satellite passes were graphed in latitude (geographic and geomagnetic), and the ground tracks were mapped with the magnetic field lines and with the locations of the magnetic and dip equators. There was no automated trough detection involved. The trough was identified by the visual inspection of the 528 Ni-Te line plot pairs. Their digital data provided the base for this study's

Table 1. Average Variation of Local Time, Magnetic Local Time, and Geographic Latitude Compiled for the Australian and American Longitude Sectors[a]

Australian Longitude Sector at 110°E (Geographic)			American Longitude Sector at 288°E (Geographic)		
LT (hours)	Latitude (Geographic) (deg)	MLT (in decimal hours)	LT (hours)	Latitude (Geographic) (deg)	MLT (in decimal hours)
12	81.2	8.78	12	81.2	13.82
11	81	8.40	11	81	13.24
10	80	8.10	10	80	12.49
9	77	7.8	9	77	11.33
8	72	7.46	8	72	9.63
7	**60**	7.00	**7**	**60**	7.64
6	**0**	6.00	**6**	**0**	5.69
5	**−60**	3.42	**5**	**−60**	5.38
4	−70	0.13	4	−70	5.29
3	−77	22.57	3	−77	5.22
2	−80	21.81	2	−80	5.13
1	−81	21.38	1	−81	5.04
0	−81.1	21.4	0	−81.1	4.95

[a]Taking some actual values from the descending F13 passes of 13 and 6, crossing the geographic equator at 110°E (geographic) in the Australian longitude sector and at 288°E in the American longitude sector, respectively, on 2 August 2000, the variation of local time (LT), geographic latitude, and magnetic local time (MLT) is illustrated. The 12 bold entries highlight that there is only a 2-h LT variation between 60°N and 60°S latitudes.

statistical analysis of the trough and subauroral Te peak. To overcome the one dimensional limitation of the individual DMSP measurements, the data were mapped across the two hemispheres by binning them into 2°(lat) × 4°(lon) cells. These map series were utilized to register the effects of the SAMA's special electrodynamics and interhemispheric plasma flows. Owing to space constraints, only one map series, constructed for the period of 28 July–7 August 2000, is presented in this paper. It is noted here that these maps track areas and regions as seen in the time-dependent spatial coordinate system of the DMSP-F13 spacecraft.

3. Observations

3.1. Underlying Magnetic Conditions

[7] The geomagnetic nature of the 2000 southern winter period investigated was probed by the three-hourly Kp indices, and by the hourly Dst and AE indices and their averaged equivalents called Dst6 and AE6. First introduced by *Werner and Prolss* [1997], an AE6 index is the weighted mean value of the previous six consecutive hourly AE indices and can be defined as

$$\mathrm{AE6} = \frac{\sum_{i=0}^{6} \mathrm{AE(UT - i[h])e^{-i}}}{\sum_{i=0}^{6} \mathrm{e^{-i}}} \qquad (1)$$

Particularly for trough studies, the usefulness of the AE6 index is related to the fact that it takes the ''memory effect'' of the ionosphere into account, as the trough position may depend on both the actual magnetic activity and the previous magnetic activity history [*Werner and Prolss*, 1997; *Prolss*, 2006, 2007]. In this study, for the first time, the Dst indices were also subjected to this averaging procedure, defined by equation (1), producing the Dst6 data. Because of the logarithmic nature of the Kp index, such an averaging procedure was not possible. However, utilizing the Kp′ index, indicating the largest Kp value during the previous 12 h, was a better option than the use of Kp index. In Figures 2a–2c, three histograms illustrate the distribution of magnetic activity level, probed by the AE6, Dst6 and Kp′ indices, during the 528 southern winter trough detections.

[8] There was a moderately disturbed 11-day period, extending from 28 July to 7 August 2000 that was chosen for presenting regional maps. The AE, Dst and Kp indices registered its magnetic activity levels (see Figures 2d–2f). Some moderate disturbance took place during the first two days (28–29 July) when the maximum AE of 1200 nT and Kp of 6-, and the minimum Dst of −71 nT were detected. Following a smaller disturbance (AE = 900 nT, Kp = 5+; Dst = −30 nT) on 31 July, there was a quieter period (1–4 August) when AE and Kp were small (∼300 nT and ∼3+) and Dst remained larger than −40 nT. After 5 August, the disturbance gradually diminished (AE ∼ 200 nT; Kp ≈ 2; Dst ≈ −20 nT) during the last two days (6–7 August).

3.2. Topside *F* Region Regional Maps

[9] A series of regional maps was constructed to illustrate the spatial distribution of plasma density (Ni), electron temperature (Te), plasma composition ($[O^+]$, $[H^+]$, $[He^+]$), plasma drifts (V_y, V_z), and plasma fluxes (F_y, F_z) in the topside ionosphere at ∼850 km altitude. In each almost global map, covering the geographic latitudes between 81°N and 81°S, the magnetic (in red) and dip (in pink) equator locations are also indicated. How the LT and MLT varied was explained in section 2.

[10] In Figures 3a and 3b, the Ni (i^+/cm^3) map illustrates the morphology of the plasma density in the topside ionosphere. According to the LT variation, the southern hemisphere received only limited sunlight at low latitudes and was in darkness at midlatitudes and high latitudes. Three major plasma density depletions ((1 to 8) • 10^3 i^+/cm^3; in dark brown) were tracked in the southern hemisphere. These are the midlatitude trough, the polar hole and an anomalously low ionization area in the SAMA region. It is mentioned here again that in this study, areas and regions indicate areas and

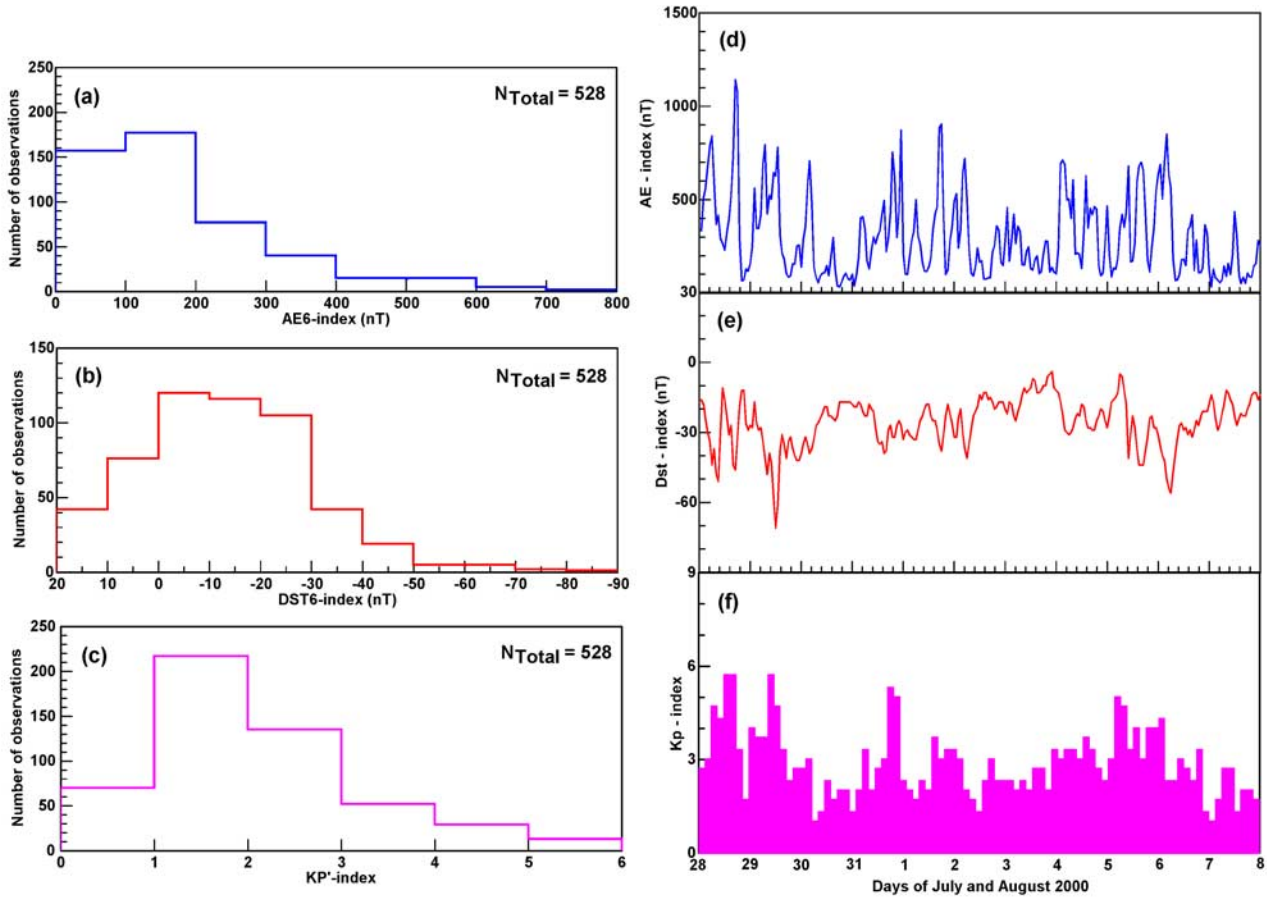

Figure 2. The histograms illustrate the detections' magnetic activity distribution probed by the (a) AE6, (b) DST6, and (c) Kp′ indices. The (d) AE, (e) Dst, and (f) Kp indices depict the geomagnetic nature of the southern winter period of 28 July–7 August 2000.

regions as seen in the time-dependent spatial coordinate system of the DMSP-F13 spacecraft. At ~55°S (geomagnetic), the trough appeared as a band of plasma depletion relative to the ionosphere both equatorward and poleward of it. When the modeled magnetic field lines were plotted over the Ni map (see right panel), it became evident that the polar hole was detected around the southern magnetic pole. Between the trough and the polar hole, a higher ion density region ((8 to 16) • 10^3 i^+/cm^3; in light brown) that is the signature of the nighttime auroral zone, can be seen. The Ni map illustrates how this ridge of auroral ionization varied with longitude. It developed best ((33 to 41) • 10^3 i^+/cm^3; in green) east of the polar hole, at longitudes situated far from the southern magnetic pole. Over the South Atlantic, the trough developed in the vicinity of the SAMA's low plasma density region. Over the northern hemisphere, the most outstanding feature is a circular shaped plasma density enhancement (>90 • 10^3 i^+/cm^3; in red) appearing over the northwestern Pacific where the morning topside ionosphere was best developed at ~6.5 LT.

[11] In Figures 3c and 3d, the electron temperature (Te; in °K) map illustrates the thermal structures of the topside ionosphere. In the southern hemisphere, a prominent band of elevated Te (>4.5 • 10^3 °K; in red and (3.8 to 4.0) 10^3 °K; in dark blue), which is the signature of a subauroral Te peak, and two well-defined regions of Te depletion ((2.0 to 2.2) • 10^3 °K; in dark brown) can be seen. A larger one is situated around the southern magnetic pole and a smaller one is located over the South Atlantic. This larger Te depletion coincides with the polar hole and indicates the absence of ionospheric heating sources as *Brinton et al.* [1978] suggested. This smaller Te depletion, situated in the SAMA region, suggests adiabatic cooling, while its northern hemisphere high Te ((4.2 to 4.5) • 10^3 °K; in pink) counterpart is the signature of adiabatic heating, and thus, these are associated with field-aligned interhemispheric plasma transport [*Venkatraman and Heelis*, 2000, and references therein]. There is also a low Te ((2.2 to 2.4) • 10^3 °K; in brown) band situated in the nighttime auroral zone. The elevated Te band in the subauroral region indicates the presence of heating sources and appears to be where the trough was tracked by the Ni map. In order to justify this assumption, the position of this Te band was determined in the Te data, and plotted over the Ni and Te maps (see right panel) revealing an excellent match that has regularly been utilized in this study to mark the Ni trough minimum. Previous and recent studies of *Kozyra et al.* [1986] and *Prolss* [2006, 2007] demonstrated the coincidence of the northern trough and subauroral Te peak, respectively.

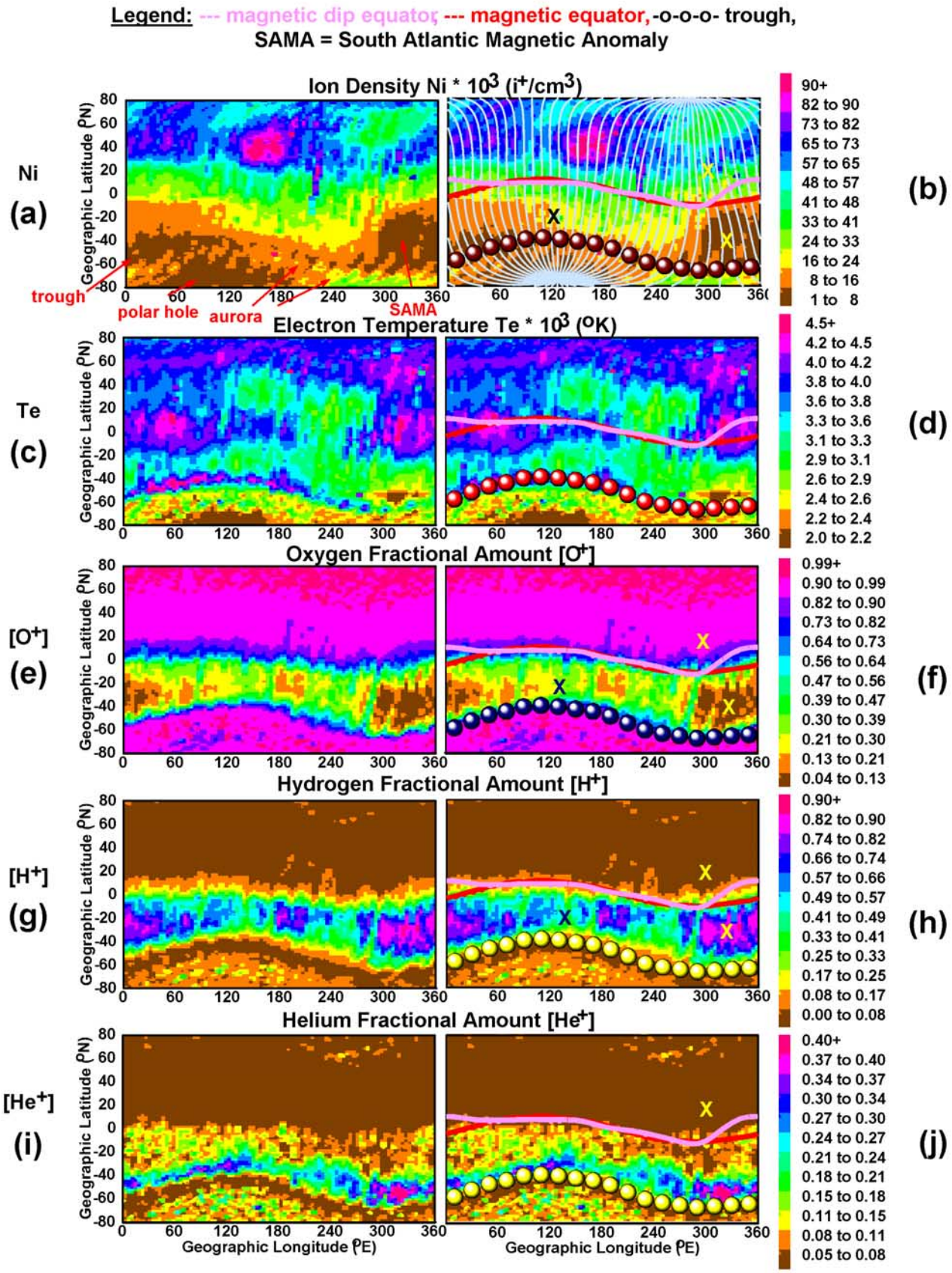
Legend: --- magnetic dip equator, --- magnetic equator, -o-o-o- trough,
SAMA = South Atlantic Magnetic Anomaly
Ion Density Ni * 10^3 (i+/cm^3)
Ni
(a)
(b)
trough
polar hole
aurora
SAMA
Electron Temperature Te * 10^3 (°K)
Te
(c)
(d)
Oxygen Fractional Amount [O+]
[O+]
(e)
(f)
Hydrogen Fractional Amount [H+]
[H+]
(g)
(h)
Helium Fractional Amount [He+]
[He+]
(i)
(j)
Geographic Latitude (°N)
Geographic Longitude (°E)
90+
82 to 90
73 to 82
65 to 73
57 to 65
48 to 57
41 to 48
33 to 41
24 to 33
16 to 24
8 to 16
1 to 8
4.5+
4.2 to 4.5
4.0 to 4.2
3.8 to 4.0
3.6 to 3.8
3.3 to 3.6
3.1 to 3.3
2.9 to 3.1
2.6 to 2.9
2.4 to 2.6
2.2 to 2.4
2.0 to 2.2
0.99+
0.90 to 0.99
0.82 to 0.90
0.73 to 0.82
0.64 to 0.73
0.56 to 0.64
0.47 to 0.56
0.39 to 0.47
0.30 to 0.39
0.21 to 0.30
0.13 to 0.21
0.04 to 0.13
0.90+
0.82 to 0.90
0.74 to 0.82
0.66 to 0.74
0.57 to 0.66
0.49 to 0.57
0.41 to 0.49
0.33 to 0.41
0.25 to 0.33
0.17 to 0.25
0.08 to 0.17
0.00 to 0.08
0.40+
0.37 to 0.40
0.34 to 0.37
0.30 to 0.34
0.27 to 0.30
0.24 to 0.27
0.21 to 0.24
0.18 to 0.21
0.15 to 0.18
0.11 to 0.15
0.08 to 0.11
0.05 to 0.08

Figure 3

[12] The topside ionosphere's plasma chemistry can be characterized by the compositions of heavy ion (O^+) and light ions (H^+, He^+). How their fractional amounts varied spatially at ~850 km altitude during the period investigated is illustrated by the maps of [O^+] (see Figures 3e and 3f), [H^+] (see Figures 3g and 3h), and [He^+] (see Figures 3i and 3j). In the right panel, the location of trough minimum is plotted over these plasma composition maps in order to get a perspective on where the Ni trough developed. In the southern hemisphere, there is a marked band of lower [O^+] ((0.75 to 0.82; in dark blue), which coincides with the Ni trough minimum indicating that the trough was a heavy-ion (Ni-O^+) trough. There is also a lower [O^+] ((0.75 to 0.82); in dark blue) area in the polar cap where the western region of the polar hole was tracked. Possibly, the eastern lower [O^+] area became canceled out in the computation process of the average [O^+] values. The [H^+] and [He^+] maps also show an interesting feature of the polar hole, that is, the [He^+] was not depleted in the topside ionosphere. *Heelis et al.* [1981] performed some modeling on the continuity dynamics of heavy and light ions under conditions characterizing the polar hole, and demonstrated that [He^+] can remain moderate at around 600 km altitude. Shown by the [H^+] and [He^+] maps, there are also well defined depletions in the [H^+] ((0.00 to 0.08); in dark brown) and [He^+] ((0.05 to 0.08); in dark brown) at trough latitudes. Illustrated in the right panel, the Ni trough minimum is situated around the equatorward edge of these coinciding [H^+] and [He^+] depletions. These composition maps clearly show that at ~850 km altitude in the topside ionosphere, the O^+ was still the dominant ion. Therefore, these [H^+] and [He^+] depletions, measured well below the heavy/light ion transition height, do not indicate the light-ion trough, which is a depletion in the electron density due to the depletion of the H^+ content at plasmaspheric altitudes where the H^+ is the dominant ion [*Moffett and Quegan*, 1983; *Rodger et al.*, 1992]. However, there is evidence [*Horwitz et al.*, 1990] that the light-ion latitudinal density profiles of the topside ionosphere sometimes show strong resembles to those of the plasmasphere. On the basis of the assumption that such resemblance existed during the period investigated, these [H^+] and [He^+] depletions can be interpreted to be the upper-ionospheric signatures of a light-ion trough. Between the dip equator and the Ni trough, the [O^+] and [H^+] varied inversely, and both display a well defined longitudinal variation that reflects the longitudinal variation of meridional and transequatorial neutral winds governed by the longitudinal variation of **B** field intensity and declination [*Titheridge*, 1995; *Venkatraman and Heelis*, 1999, 2000]. Where the combination of poleward directed neutral winds and interhemispheric (winter) downward flows maximized, there were prominent [O^+] lows and [H^+] highs such as at ~30°E, ~70°E, ~110°E, ~180°E (geographic). Over the South Atlantic, the maximum winter downward flow was accelerated by the SAMA effects. These detections at these locations are consistent with the results of *Kutiev et al.* [1980]. Those authors, utilizing the Ogo-6 satellite data (recorded between 800 km and 1090 km), also detected this longitude-dependent [O^+]-[H^+] pattern at midlatitudes during southern winter (in July 1969) at local midnight and explained them with the winds' effects. Elsewhere, like at 130°E, the weaker net downward drifts left the heavy ions at higher altitudes and at low recombination rates, leaving their concentrations at midlatitudes minimum 7 times higher (Ni ≈ (8–16) • 10^3 i^+/cm^3; in light brown and Ni≈(16–24) • 10^3 i^+/cm^3; in yellow; [O^+] ≈ 0.21–0.30 in yellow) than in the SAMA region. There, the strongly impeded return flow of H^+ created a light ion concentration ([H^+] ≈ 0.33–0.41 in green; see Figure 3h) that was only a third of the [H^+] in the SAMA region. It is noted here that in the northern daytime hemisphere, the heavy-ion ([O^+]) content (0.9 to 0.99) and the light-ion ([H^+]-[He^+]) content (0.00 to 0.08 and 0.05 to 0.08, respectively) varied also inversely, but remained spatially uniform because of the small declination angles introducing little longitudinal variations [*Titheridge*, 1995].

[13] Cross-track plasma drifts and fluxes are useful indicators of plasma movements in the vertical and horizontal directions. Along the vertical Z axis, plasma fluxes can image vertical plasma flows such as upward (+) and downward (−) flows (away from and toward the center of the Earth, respectively). Along the horizontal *y* axis, they can image horizontal plasma convections in the eastward (+) and westward (−) directions (left is + in the direction of the spacecraft's travel).

[14] In Figures 4a and 4b the vertical plasma drifts (V_Z in m/s) and in Figures 4c and 4d the vertical plasma fluxes (F_Z in [$i^+/(cm^2s)$]) are mapped over the two hemispheres. Large upward (+) plasma drifts ((18 to 70) m/s in pink; >70 m/s in red) and flows ((63 to 120) • 10^7 [$i^+/(cm^2s)$] in pink; >120 • 10^7 [$i^+/(cm^2s)$] in red) are indicated just north of the dip equator and in both hemispheres' aurora zones. The largest low-latitude maximum upward drifts occurred in the American longitude sector and the most intensive downward drifts ((−500 to −448) m/s in dark brown) were tracked over the SAMA region. These northern (summer) upward and southern (winter) downward drifts indicate field-aligned interhemispheric plasma flows that reached their seasonal (southern winter) maximum over the Atlantic, as the study of *Venkatraman and Heelis* [2000] revealed. In good agreement with the study of *Venkatraman and Heelis* [1999], the associated adiabatic (northern summer) heating and (southern winter) cooling effects of the plasma was tracked by the Te map. However, this V_Z map clearly illustrates these field-aligned plasma flows' strong hemispherical asymmetry. This was due to the SAMA's special electrodynamic effects (see details in section 1) that created also a strong downward drift over the South Atlantic, which, in turn, enhanced the interhemispheric (winter) downward diffusion. The affected region was registered by this net maximum downward drift that marked the SAMA's high-conductivity region. Its alignment is indicated by a pink broken line plotted over the V_Z map. Details will be discussed below and in section 5.2. Meanwhile, smaller downward (−) velocities were detected ((−85

Figure 3. The regional maps depict the spatial distribution of (a and b) ion density (Ni in 10^3 • i^+/cm^3) and (c and d) electron temperature (Te in 10^3 • °K), and the fractional amounts of (e and f) [O^+], (g and h) [H^+], and (i and j) [He^+] in the topside ionosphere during the southern winter period of 28 July–7 August 2000. The x symbols indicate the regions where the numerical data were quoted from.

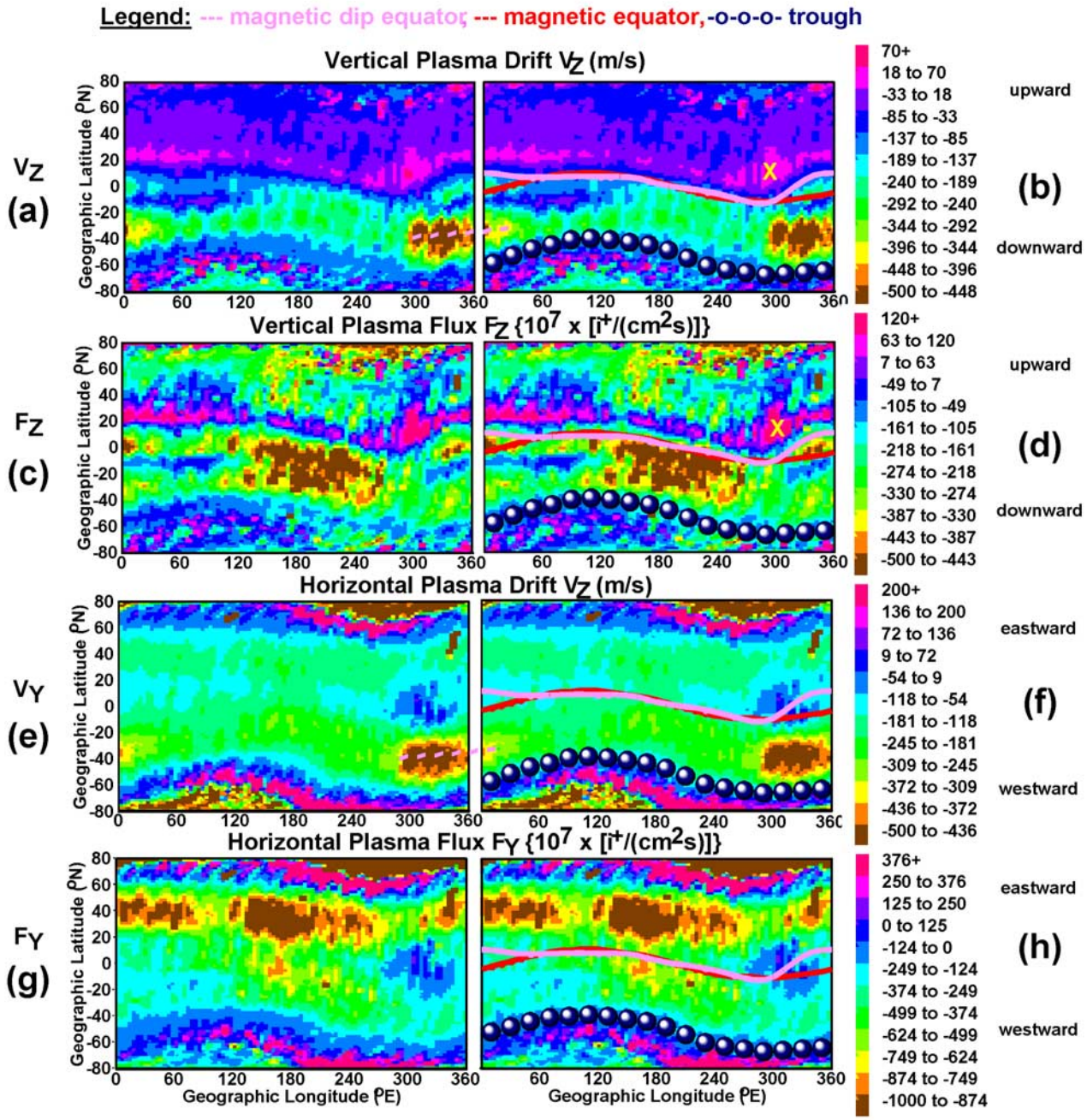

Figure 4. The regional maps depict the spatial distribution of (a and b) vertical plasma drift (V_Z in m/s), (c and d) vertical plasma flux (F_Z in $\{10^7 \bullet [i^+/(cm^2s)]\}$), (e and f) horizontal plasma drift (V_Y in m/s), and (g and h) the horizontal plasma flux (F_Y in $\{10^7 \bullet [i^+/(cm^2s)]\}$). The x symbols indicate the regions where the numerical data were quoted from. The pink broken lines indicate the hypothetical location of the east-west conductivity gradient.

to −33) m/s in dark blue; and [(−137 to −85) m/s in blue) over the dip equator. On the basis of the experimental and modeling studies of *Balan et al.* [1998, 2008, and references therein], net vertical drift velocities in the vicinity of the dip equator are due to the combined effects of vertical $\mathbf{E} \times \mathbf{B}$ drifts, neutral winds and other dynamic sources such as tides and waves. There, the equatorward (poleward) meridional neutral winds can provide a vertical upward (downward) drift velocity component. In this study, the poleward directed neutral winds moved the plasma down the magnetic field lines and provided a vertical downward drift velocity that added to the vertical $\mathbf{E} \times \mathbf{B}$ drifts. However, at around this time of the year, the apex height of the flux tubes, on which the interhemispheric plasma transport occurs, is at around the 850 km altitude of the DMSP spacecraft [*Venkatraman and Heelis*, 2000]. Thus, the transequatorial winds could also affect the equatorial vertical drifts by introducing an upward drift at low northern latitudes and a downward drift at low southern latitudes. These additional upward/downward drifts could impede/accelerate the local vertical downward drifts.

This study's V_Z map tracked the net vertical drifts. Utilizing the ROCSAT-1 database, recorded at ~600 km altitude, *Fejer et al.* [2008] obtained accurate quiet time **E** × **B** drift values by excluding unrealistic measurements, and documented the average variation of vertical **E** × **B** drift between around −30 m/s and 40 m/s with LT during the southern winter months. This study's V_Z map tracked the net effects of the hemispheric and interhemispheric plasma flows on the vertical **E** × **B** drift, as the apex height was at the altitude of the F13 spacecraft. Thus, this study's equatorial vertical drift velocities are net values and not unrealistic vertical **E** × **B** drift velocities. Over the Pacific, the interhemispheric plasma flows created strong upward ((63 to 120) • 10^7 [i^+/(cm^2s)] in red) and downward ((−500 to −443) • 10^7 [i^+/(cm^2s)] in dark brown) plasma fluxes (see Figures 4c and 4d). At southern trough latitudes, the small negative drift and flux values ((−85 to −33) m/s and (−49 to 7) • 10^7 [i^+/(cm^2s)] in dark blue) indicate slow vertical downward drifts and flows, respectively. These are illustrated with the location of the elevated Te band (indicating the trough minimum) plotted over these V_Z and F_Z maps (see right panel) showing an accurate coincidence. There are also well defined zones of medium strong downward drifts ((−344 to −292) m/s in green) and flows ((−105 to −49) • 10^7 [i^+/(cm^2s)] in blue; (−161 to −105) • 10^7 [i^+/(cm^2s)] in light blue) in the polar hole.

[15] The spatial distribution of horizontal plasma drifts (V_Y in m/s) and plasma fluxes (F_Y in [i^+/(cm^2s)]) are shown in Figures 4e and 4f and Figures 4g and 4h, respectively. At trough latitudes, the F_Y map tracked very slow westward plasma fluxes ((−124 to 0) • 10^7 [i^+/(cm^2s)] in blue), indicating flow stagnations. This will be further demonstrated with line plots later in this paper. The detection of the stagnating plasma at the heavy-ion (Ni-O^+) trough minimum is demonstrated with the right panel maps indicating that this heavy-ion trough was a stagnation trough. Some weak westward plasma flows ((−124 to 0) • 10^7 [i^+/(cm^2s)] in blue; (−249 to −124) • 10^7 [i^+/(cm^2s)] in light blue) were detected in the polar hole indicating slow plasma circulations. In both hemispheres, at auroral latitudes, the V_Y and F_Y maps tracked the strongest eastward (+) plasma drifts (>200 m/s; in red) and flows (>376 • 10^7 [i^+/(cm^2s)] in red), respectively. Meanwhile, the strongest westward (−) plasma drifts ((−500 to −436) m/s; in dark brown) were detected in the SAMA region, and in the northern and southern polar caps. In the SAMA region, this westward drift is the westward (horizontal, cross-track) component of the net field-aligned downward plasma flows. As the field-aligned interhemispheric downward drift was accentuated by the SAMA's electrodynamics, these maximum net westward drifts also registered the SAMA's high-conductivity region. Its magnetic alignment is obvious, as the pink broken line plotted over the V_Y map indicates. Furthermore, these strong net westward drifts transported the plasma away from the SAMA's high-conductivity region and contributed to the creation of a low plasma density region that was tracked by the Ni map very accurately also over the same region, that is, the SAMA's high-conductivity region.

3.3. Topside *F* Region Latitudinal Profiles and Spectrograms

[16] Utilizing Ni-Te line plot pairs and spectrogram images, two figures are constructed to illustrate the major morphological features of the nighttime topside ionosphere, under quiet magnetic conditions (Kp ≤ 3), in the various longitude sectors. After inspecting visually the modeled magnetic field lines and the ground tracks of the F13 passes providing the data, and employing various Stanford Graphics plotting tools, the alignment of the F13 passes were identified within an accuracy of around ±2° (lat). The automatically marked spectral images provided information, based on the classification of *Newell et al.* [1996], on the structured particle precipitation regimes and on the location of the plasmapause.

[17] Shown in the global map of Figure 5, the southbound F13 passes provided field-aligned detections over the southwestern (see pass 10) and southeastern Pacific (see pass 6). However, the ground tracks were positioned perpendicular to the magnetic field lines at trough latitudes over the Indian Ocean and in the Australian sector (see pass 13), and at high latitudes over the South Atlantic (see pass 1). The significance of field-aligned observations is related to the facts that the geomagnetic field plays a key role in the dynamics of the ionospheric plasma and therefore in the formation of the midlatitude trough and polar hole, that the subauroral Te peaks are created by field-aligned heat flows, and that the plasma at midlatitudes is transported along the magnetic field lines. Thus, the field-aligned observations show the true cross sections of the ionospheric features. In this study, only field-aligned cross sections were utilized to define the equatorward and poleward trough boundaries, and their characteristics. Two examples are illustrated in Figures 5a and 5b.

[18] Shown in Figure 5a, a better developed trough was detected over the southwestern Pacific. There, the magnetic equator appears north of the geographic equator, and their offset increases westward. Because of this, mid magnetic latitudes are situated at higher geographic latitudes. The trough was tracked at ~45°S–50°S geographic (~57°S; geomagnetic). The equatorward neutral winds were most efficient in keeping the solar produced ionization at high altitudes and at low recombination rates. This field-aligned Ni-Te line plot pair illustrates the basic plasma density and thermal structures of a quiet time southern winter trough (at ~5 LT) and polar hole (at ~2 LT), and some auroral ionization separating them (at ~4.5 LT). The generally inverse relationship between the electron temperature and the plasma density, particularly at trough latitudes where the electron temperatures became elevated and formed a well defined subauroral Te peak (~5000°K) that can be regarded as a very accurate marker of the trough minimum, is obvious. Meanwhile, the Te suddenly decreased in the aurora region and became a minimum (~1500°K) in the polar hole that appeared as a cavity of ionization over the polar cap. Because of the structured plasma around the trough, the equatorward and poleward trough boundaries were not always obvious. However, their Te signatures were more apparent. Both trough boundaries were indicated by a Te-gradient change from shallower to steeper toward the trough minimum (see also Figure 5b). At the polar hole's steep equatorward wall, created by the poleward edge of the aurora, the Te also peaked. The polar hole appeared with a broad minimum that exhibited little plasma density variations. An interesting feature is that the field-aligned pass 10 crossed the southern magnetic pole.

[19] Over the southeastern Pacific, the field-aligned Ni profile of Figure 5b detected the trough in a less developed

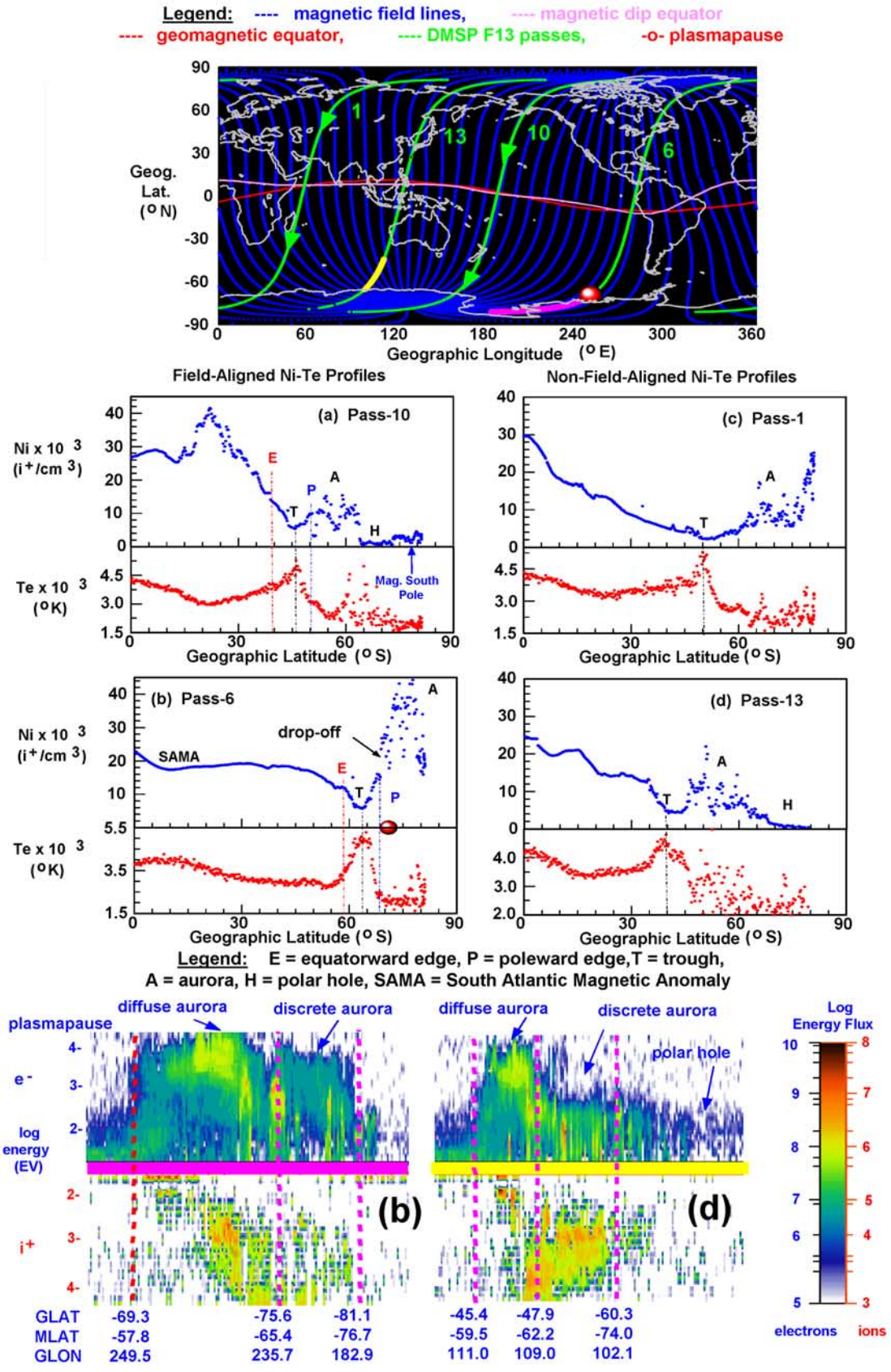
Legend: ---- magnetic field lines, ---- magnetic dip equator
---- geomagnetic equator, ---- DMSP F13 passes, -o- plasmapause
Geog. Lat. (°N)
Geographic Longitude (°E)
Field-Aligned Ni-Te Profiles
Non-Field-Aligned Ni-Te Profiles
(a) Pass-10
(c) Pass-1
(b) Pass-6
(d) Pass-13
Ni x 10 3 (i+/cm 3)
Te x 10 3 (°K)
Mag. South Pole
drop-off
SAMA
Geographic Latitude (° S)
Legend: E = equatorward edge, P = poleward edge, T = trough,
A = aurora, H = polar hole, SAMA = South Atlantic Magnetic Anomaly
plasmapause
diffuse aurora
discrete aurora
polar hole
e-
log energy (EV)
i+
(b)
(d)
Log Energy Flux
electrons
ions
GLAT -69.3 -75.6 -81.1 -45.4 -47.9 -60.3
MLAT -57.8 -65.4 -76.7 -59.5 -62.2 -74.0
GLON 249.5 235.7 182.9 111.0 109.0 102.1

Figure 5

form at ~67°S (geographic). There, the magnetic equator is situated in the southern hemisphere and mid magnetic latitudes are situated at higher geographic latitudes. At mid geographic latitudes, the solar produced plasma became depleted during the night owing to the downward diffusion created by the interhemispheric plasma flows and to the SAMA effects (see details in section 5.2). Because of these, the plasma density on the trough equatorward side (at ~58°S, geographic) was low (~11.5 • 10^3 i^+/cm^3) relative to the trough minimum (~5.5 • 10^3 i^+/cm^3), only 2× higher. Owing to this small difference, only ~6 • 10^3 i^+/cm^3, the trough appeared with a small but well defined equatorward edge and wall. Its Te profile, showing less scatter, depicts very clearly the above described gradient increases toward the trough minimum. These Ni-Te plots also demonstrate that the temperature remained a constant maximum throughout the narrow trough minimum that was ~3°–5° (lat) in width. This constant Te suggests no Te-gradient related instabilities in the trough minimum, while the plasma can be unstable to temperature gradient instabilities in both trough walls [*Rodger and Aarons*, 1988]. *Rodger* [1984] confirmed experimentally that the trough minimum is a region where instabilities are rare. On the basis of the also field-aligned spectrogram image (see pink track in the global map and also bottom panels), the auroral plasma enhancements were the signature of a diffuse and a discrete aurora, and the electron and ion precipitation events ceased in the polar hole. During this period of increasing magnetic activity, the plasmapause and its ionospheric signature, a Ni dropoff (its location is indicated by a red dot), were also tracked by this field-aligned spectrogram image and Ni plot, respectively, at ~7.25° away from the trough minimum, on the equatorward side of the diffuse auroral increases. The plasmapause position is also plotted in the global field-line map. Combining these field-aligned Ni-Te line plots with the also field-aligned spectrogram image provided the ability to relate electron density structures to particle precipitations, and to define the position of the plasmapause independently and simultaneously. Thus, this field-aligned observation demonstrates the relationship of the tracked Ni trough to the observed plasmapause during an increasing magnetic activity period, and reveals with a ~95% certainty their development on the same magnetic field line. Utilizing global observations, the recent studies of *Yizengaw and Moldwin* [2005] and *Yizengaw et al.* [2005] correlated the trough and the plasmapause, and proved with no modeled magnetic field lines that these occur on the same magnetic field line. Following that, those authors compared the latitudes of the trough and plasmapause without utilizing any modeled magnetic field lines.

[20] In Figure 5c, a non-field-aligned pass depicts a distorted Ni cross section of the trough exhibiting a broad minimum and the aurora. The exact location of the trough minimum in this low plasma density region (~2.3 • 10^3 i^+/cm^3) is indicated by the subauroral Te peak. This example also demonstrates that the non-field-aligned Te detections, although they are quite scattered at auroral latitudes, still depict the above described inverse relationship between the Ni and Te.

[21] When a DMSP pass is aligned at trough latitudes perpendicular to the magnetic field lines, it can also provide a scientifically meaningful detection of the trough. Such detection is shown in Figure 5d depicting a short (~4°) section of the trough's length in the NE–SW (geographic) direction in the Australian longitude sector. There, the trough appeared at ~5.5 LT with some ionization enhancement that was associated with auroral precipitation (at ~5 LT) and the polar hole occurred at ~2.5 LT. The location of the exact trough minimum is marked by the subauroral Te peak. On the basis of the spectrogram image (see yellow track in the global map and also bottom panels), the auroral plasma enhancements are the signature of a diffuse and a discrete aurora, and the electron and ion precipitation events ceased in the polar hole.

[22] Figure 6 illustrates the region of the SAMA. Two passes (see Figures 6a and 6b), tracking its central region (~22.8 • 10^3 nT [*Trivedi et al.*, 2005]) on 2 August 2000, show some very low plasma densities (3.5–5.7 • 10^3 i^+/cm^3) between ~30°S and ~60°S. Over the South Atlantic, the trough developed poleward of this low Ni region in its least developed form because of the low background ionization equatorward of it. There, in the already anomalously low plasma densities, formed by the combination of hemispheric and interhemispheric downward drifts and the SAMA's own high conductivity (see details in section 5.2), the trough created an additional plasma depletion. At the trough's equatorward edge (see Figure 6b), the plasma density was very low (~5.7 • 10^3 i^+/cm^3) relative to the trough minimum (~3.7 • 10^4 i^+/cm^3), only 1.5× higher. Because of this small difference, only ~4 • 10^3 i^+/cm^3, the trough appeared almost without an equatorward edge and wall. A well developed diffuse aurora created the trough's steep poleward wall, as shown by the spectrogram image (its location is indicated by the pink track in the global map). Between 60°S and 81°S, the high-latitude section of the first pass (see Figure 6a) is aligned perpendicular to the magnetic field lines. This provides a nice plasma density profile of the trough and the spectrogram image depicts two well defined electron precipitation edges with an offset of ~5°. At 67.6°S, the first edge represents the first point at which the precipitation was above the noise level. At 72.5°S, the second edge is the zero energy electron boundary [*Newell et al.*, 1996]. The third pass (see Figure 6c), which is field-aligned at southern midlatitudes and high latitudes, tracked over the South American continent the western section of the SAMA region. Equatorward of the trough, where the magnetic field is not anomalously low (30.0–35.0 • 10^3 nT [*Trivedi et al.*, 2005]), the plasma

Figure 5. (top) The global map illustrates the ground tracks of F13 passes shown below, the magnetic field lines, and the magnetic and dip equators. (a and b) Two field-aligned plasma density-electron temperature (Ni-Te) line plots show the midlatitude trough (Figures 5a and 5b), the nighttime auroral zone (Figures 5a and 5b), the polar hole (Figure 5a), and the related thermal structures. (c and d) A non-field-aligned Ni-Te line plot pair (Figure 5c) depicts distorted trough and subauroral Te peak detections. A Ni-Te line plot pair, aligned perpendicular to the magnetic field lines, shows a short longitudinal section of the trough region and its thermal structures. (bottom) Two spectrograms show the structured particle precipitation regions of the nighttime auroral zones (Figures 5b and 5d). The geographic (GLAT) and magnetic (MLAT) latitudes are in °N, and the geographic longitudes (GLON) are in °E.

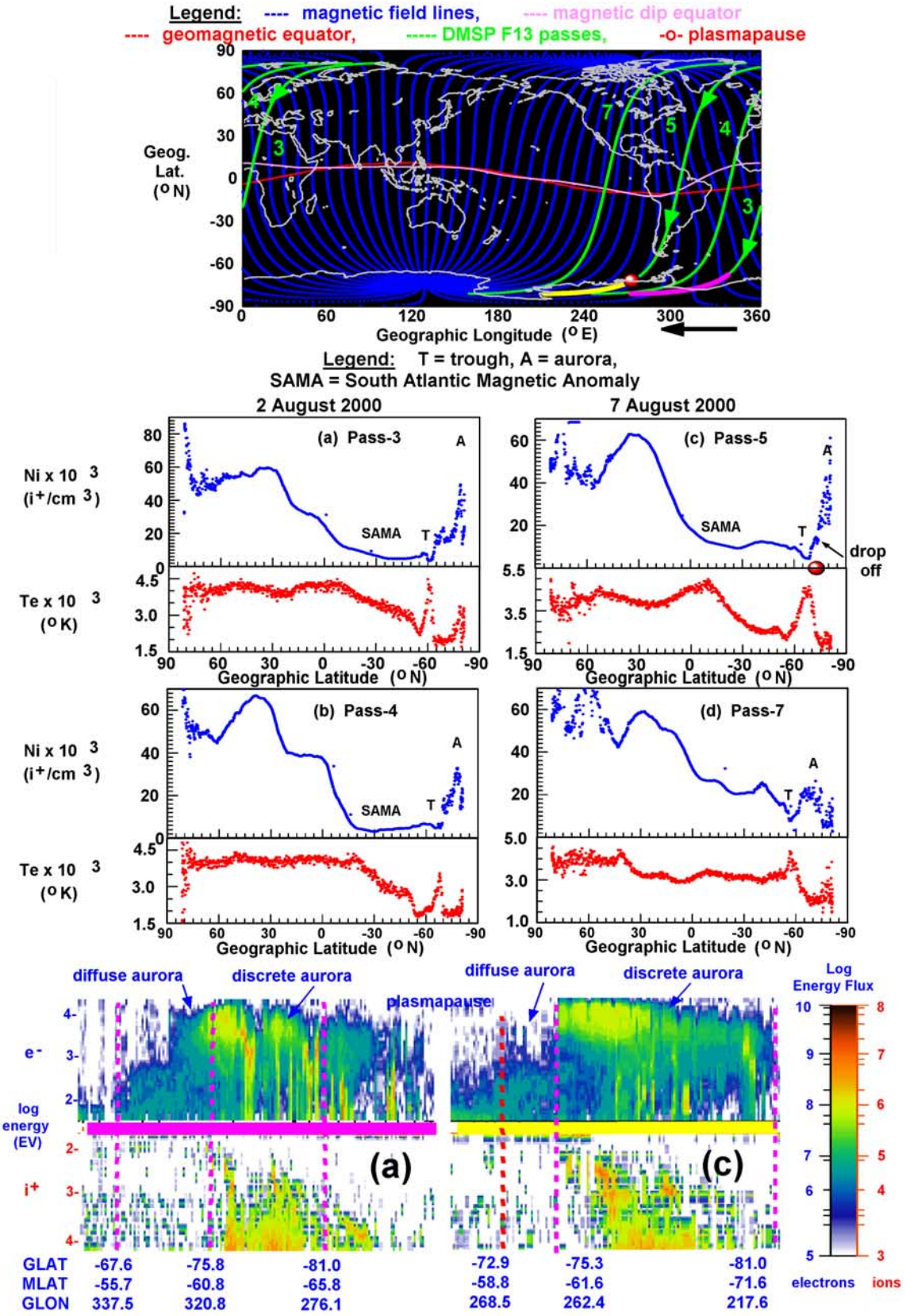
Legend: ---- magnetic field lines, ---- magnetic dip equator
---- geomagnetic equator, ----- DMSP F13 passes, -o- plasmapause
Geog. Lat. (°N)
Geographic Longitude (°E)
Legend: T = trough, A = aurora,
SAMA = South Atlantic Magnetic Anomaly
2 August 2000
7 August 2000
(a) Pass-3
(b) Pass-4
(c) Pass-5
(d) Pass-7
Ni x 10 3 (i+/cm 3)
Te x 10 3 (°K)
SAMA
drop off
Geographic Latitude (°N)
diffuse aurora
discrete aurora
plasmapause
Log Energy Flux
e-
log energy (EV)
i+
electrons
ions
GLAT -67.6 -75.8 -81.0 -72.9 -75.3 -81.0
MLAT -55.7 -60.8 -65.8 -58.8 -61.6 -71.6
GLON 337.5 320.8 276.1 268.5 262.4 217.6

Figure 6

densities were considerably higher (twice as large, ~11.5 • 10^3 i^+/cm^3) at ~45°S. The trough appeared with a moderately steep equatorward wall, its poleward wall was almost vertical. Detected as a Ni dropoff, the plasmapause developed at ~4.5° away from the trough minimum. This pass's field-aligned spectrogram (see yellow track and also bottom panels) also detected the plasmapause (its location is indicated by a red dot) on the equatorward side of the diffuse auroral increases. Just outside the SAMA region, a field-aligned pass (see Figure 6d) tracked significantly larger plasma densities at midlatitudes (~20.6 • 10^3 i^+/cm^3), equatorward of the trough. All the Te profiles show the subauroral Te peak (~4000°K), marking very accurately the trough minimum, and the region of minimum Te (~1600°K – ~2500°K) in the aurora zone.

[23] All these passes demonstrate that it is vital to know both the location of and the alignment of the ground tracks with respect to the magnetic field lines, when plasma density features are investigated. It is also obvious that the accurate location of the trough minimum can be identified by any of the Ni-Te line plots, regardless of the alignment of the pass's ground track. As this study's database contains only ~10% field-aligned passes, the trough features such as the trough boundaries could not be investigated statistically. *Brinton et al.* [1978] obtained O^+-Te profiles from the AE-C data, and the Dynamics Explorer-2 spacecraft provided the electron density (Ne) and Te data for the studies of *Rodger et al.* [1992] and *Prolss* [2006, 2007]. Similarly to this study, those authors utilized satellite passes cutting through latitudes and longitudes, and thus detected the trough in varying LT and MLT. However, in this study, the modeled magnetic field lines permitted the identification of the field-aligned observations and only such observations were utilized to describe the morphology of the trough and polar hole. As those studies did not show any modeled magnetic field lines and ground tracks, it is not known which detections were field-aligned.

[24] In Figure 7, two field-aligned latitude cross sections are prepared with the Ni, Te, $[O^+]$, $[H^+]$ and $[He^+]$ data from their respective maps for the geographic longitudes of 120°E and 312°E. At both longitudes, these field-aligned line plots depict the Ni trough, the Ni auroral enhancement, the steep $[O^+]$ gradient at the Ni trough minimum, and the upper ionospheric signatures of the light-ion trough. Although there is little resemblance between the Ni trough and the upper ionospheric signatures of the light-ion trough, their coincidence at both longitudes is evident. At 120°E, the signature of the polar hole is also well recognizable in the $[H^+]$, but not in the $[He^+]$, and the $[H^+]$ signature is very similar to the Ni signature. At 312°E, the plots also depict the northern Ni enhancement created by the summer upward flows, and the anomalously low Ni and $[O^+]$ created by the combination of winter downward flows and SAMA effects. Here, the $[H^+]$ was high and $[He^+]$ varied.

[25] Figure 8 is constructed for the southern hemisphere only. It illustrates four Ni-Te profiles, some of them were shown previously, with their vertical (Z) and horizontal (Y) plasma drift (V) and flux (F) profiles. The magnetic field-line map shows the ground tracks of the passes providing the data and the detected trough minimum locations. One pass (pass 6) is entirely field-aligned and one pass (pass 10) is very close to the field line. At trough latitudes, the V_Y and V_Z plots show the slightly increased plasma velocities. *Prolss* [2007] also detected similar V_Z features over the northern hemisphere. Meanwhile, the F_Y plots depict the plasma stagnation events and how these events varied with longitude. Interestingly, the plasma stagnation was most prominent in the South Atlantic, where the convective $\mathbf{E} \times \mathbf{B}$ plasma flows were strongest because of the SAMA effects. On the basis of the plasma drift velocity expression of $\mathbf{E} \times \mathbf{B}/B^2$ [*Kendall and Pickering*, 1967], the plasma drift is expected to be larger that usual in the SAMA region owing to the weak **B** field and strong **E** field there (see details in section 5.2). In good agreement with this, larger than usual V_Z and V_Y drifts tracked in the SAMA. Meanwhile, two F_Y plots, from passes 13 and 10, detected the slow plasma flows in the polar hole. An interesting feature is that the non-field-aligned pass 3 detected the highest midlatitude (~35°S) net V_Z and V_Y plasma drifts over the anomalously low Ni region. During the 1991 southern winter, *Venkatraman and Heelis* [2000] detected maximum interhemispheric downward plasma drifts at lower latitudes, at ~17°S (magnetic) in this longitude sector at 21 MLT. Their V_Z plot shows how quickly the downward drift returned to zero, on both sides, at ~30°S and ~5°S latitudes. This study's V_Z plot illustrate that the downward diffusion peaked at higher latitudes, at ~30.2°S (geographic) or ~36.4°S (geomagnetic) at ~5.5 LT (~5.5 MLT). Because of the development of the SAMA's high-conductivity region, the SAMA's electrodynamic effects kept the downward drift close to maximum over the South Atlantic. As was shown before, the V_Z and V_Y maps of Figure 4 tracked the regions of maximum net drifts over the South Atlantic.

4. Statistical Results

[26] All the 528 Ni-Te profiles were checked visually. When there was a doubt regarding the signature of the trough minimum, the V_Z and F_Y data that tracked other trough signatures (such as the increased vertical upward drift at the trough minimum and the stagnating plasma) were inspected. Utilizing the digital data, the coinciding locations of the trough minimum and subauroral Te peak were identified, and recorded with all the other measured values. These data, containing no false identifications, provided the base for a statistical study. Its aim was to correlate both the location (in geomagnetic latitude (MLAT)) and the magnitude of the subauroral Te peak with the geomagnetic activity. On the basis of the studies of *Werner and Prolss* [1997] and *Prolss* [2006, 2007], the use of AE6 index, accounting for the "memory effect" (see details in section 1), was recognized and adopted. For the same reason, the Kp′ and Dst6 values

Figure 6. (top) Same as for Figure 5. (a–d) The plasma density-electron temperature (Ni-Te) line plots show the plasma density structures in the SAMA region (Figures 6a–6c) and just outside of it (Figure 6d), and the related thermal structures. (bottom) Two spectrograms show the structured particle precipitation regions of the nighttime auroral zones tracked perpendicular to the magnetic field lines (Figure 6a) and along the magnetic field line (Figure 6c). The geographic (GLAT) and magnetic (MLAT) latitudes are in °N, and the geographic longitudes (GLON) are in °E.

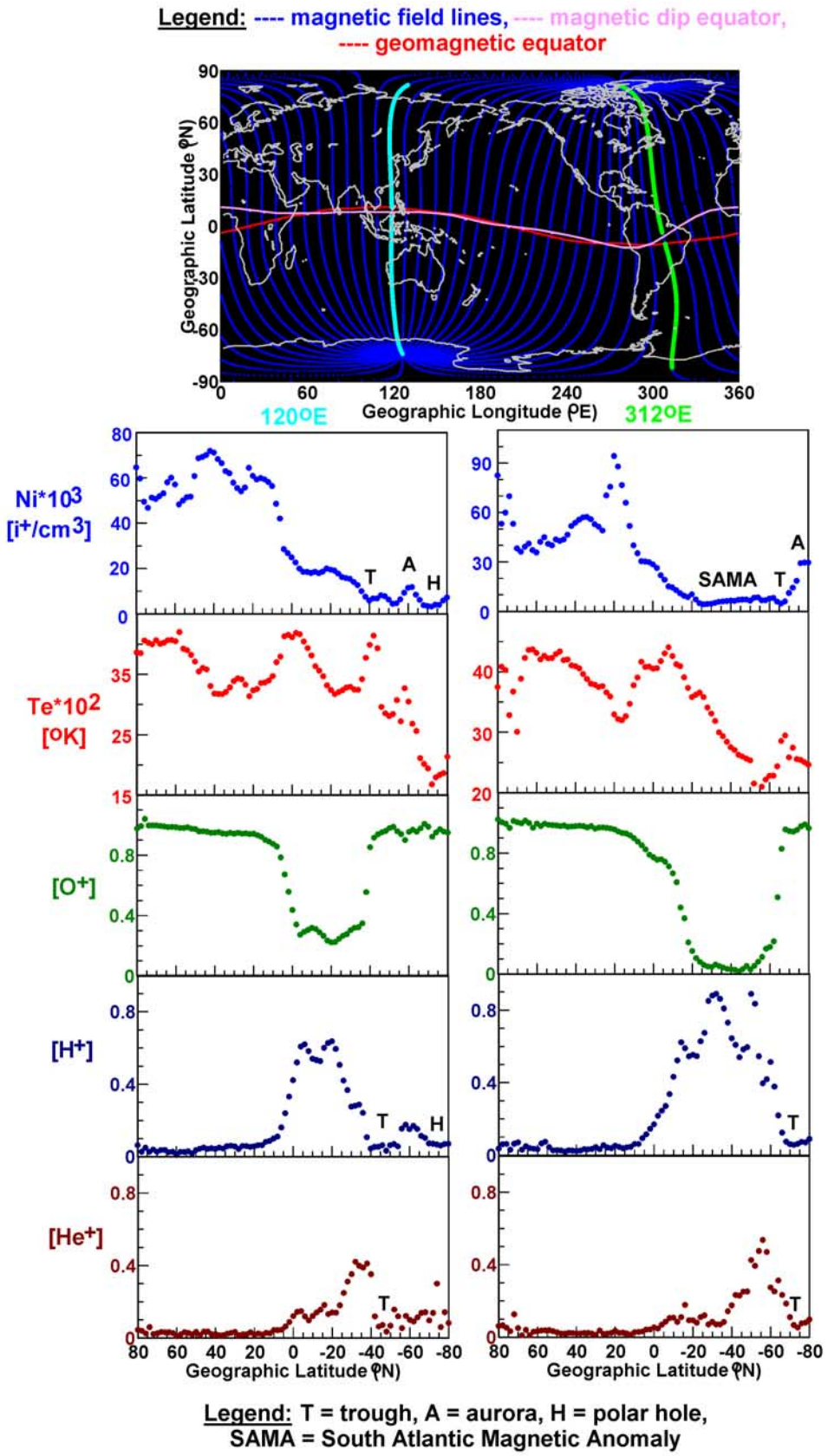
Legend: ---- magnetic field lines, ---- magnetic dip equator,
---- geomagnetic equator
Geographic Latitude (°N)
Geographic Longitude (°E)
120°E
312°E
Ni*10^3 [i+/cm3]
Te*10^2 [°K]
[O+]
[H+]
[He+]
T
A
H
SAMA
Geographic Latitude (°N)
Legend: T = trough, A = aurora, H = polar hole,
SAMA = South Atlantic Magnetic Anomaly

Figure 7

were utilized instead of the Kp and Dst indices (see details in section 1). In Figure 9, a series of error bar plots illustrate the results of these correlations performed on the MLAT (see Figures 9a–9c) and on the magnitude of the subauroral Te peak (see Figures 9d–9f). A median value with a ± error was obtained for each sampling interval. The linear nature of the plots is obvious. A line of best fit for the median values of each plot was produced, and the associated parameters such as a and b, defining the intersection of the ordinate and the slop of the regression line, respectively, were identified with a maximum and minimum value. For each parameter, a ± error, indicated as Δa and Δb, was computed from these maximum and minimum values. These parameters permitted the modeling of these linear variations as $y(x) = a \pm b(x)$ with statistical errors. For each case, a model describing this linear relationship between 3 MLT and 6 MLT was produced.

$$\begin{gathered}\mathrm{MLAT(AE6)[^\circ S]} = 57.47[^\circ\mathrm{S}] - 0.014[^\circ\mathrm{S/nT}]\mathrm{AE6} \\ \Delta a = \pm 3.19[^\circ\mathrm{S}] \qquad \Delta b = \pm 0.003[^\circ\mathrm{S/nT}]\end{gathered} \tag{2}$$

$$\begin{gathered}\mathrm{MLAT(KP')[^\circ S]} = 58.48[^\circ\mathrm{S}] - 2.156[^\circ\mathrm{S}]\mathrm{KP'} \\ \Delta a = \pm 3.34[^\circ\mathrm{S}] \qquad \Delta b = \pm 0.332[^\circ\mathrm{S}]\end{gathered} \tag{3}$$

$$\begin{gathered}\mathrm{MLAT(DST6)[^\circ S]} = 56.00[^\circ\mathrm{S}] + 0.051[^\circ\mathrm{S/nT}]\mathrm{DST6} \\ \Delta a = \pm 3.71[^\circ\mathrm{S}] \qquad \Delta b = \pm 0.009[^\circ\mathrm{S/nT}]\end{gathered} \tag{4}$$

$$\begin{gathered}\mathrm{Te(AE6)[^\circ K]} = 3991.89[^\circ\mathrm{K}] + 1.315[^\circ\mathrm{K/nT}]\mathrm{AE6} \\ \Delta a = \pm 443.71[^\circ\mathrm{K}] \qquad \Delta b = \pm 0.444[^\circ\mathrm{K/nT}]\end{gathered} \tag{5}$$

$$\begin{gathered}\mathrm{Te(KP')[^\circ K]} = 3791.12[^\circ\mathrm{K}] + 233.091[^\circ\mathrm{K}]\mathrm{KP'} \\ \Delta a = \pm 309.56[^\circ\mathrm{K}] \qquad \Delta b = \pm 65.63[^\circ\mathrm{K}]\end{gathered} \tag{6}$$

$$\begin{gathered}\mathrm{Te(DST6)[^\circ K]} = 4099.35[^\circ\mathrm{K}] - 10.226[^\circ\mathrm{K/nT}]\mathrm{DST6} \\ \Delta a = \pm 326.03[^\circ\mathrm{K}] \qquad \Delta b = \pm 1.355[^\circ\mathrm{K/nT}]\end{gathered} \tag{7}$$

5. Discussion

5.1. Midlatitude and High-Latitude Plasma Density and Thermal Morphology

[27] In the midlatitude and high-latitude regions, most large-scale plasma depletion structures are present when the ionosphere receives little or no solar illumination [*Rodger et al.*, 1992]. During that time, at F region heights, a depletion in electron concentration usually implies a depletion of the $[O^+]$. At subauroral and higher latitudes, these Ni-$[O^+]$ depletions correspond to a heavy-ion midlatitude trough and a polar hole, respectively [*Brinton et al.*, 1978].

[28] This study's Ni and $[O^+]$ maps offered the ability to track simultaneously and independently the large-scale structures in the heavy ion (Ni-O^+) plasma concentrations of the nighttime topside ionosphere. These maps have revealed the coincidence of the Ni and O^+ features of the trough (at ~55°S; geomagnetic) and polar hole. These findings are similar to the results of *Brinton et al.* [1978], although they mapped the trough with other high-latitude features in polar MLT-Λ (magnetic local time–invariant latitude) plots. Those authors also demonstrated with a series of line plots that the O^+ plasma component was the dominant ion at ~300 km. This study's high-resolution maps, obtained with in situ data recorded at ~850 km altitude, have demonstrated that the O^+ component was still the dominant ion at ~850 km at trough latitudes and poleward, and tracked a heavy-ion (Ni-O^+) trough, a polar hole and a SAMA related large-scale heavy-ion depletion (see details in section 5.2) in the topside ionosphere during the 2000 southern winter.

[29] These Ni and O^+ maps coupled with the Te map, and the individual Ni-Te profiles tracked elevated electron temperatures at trough latitudes that have provided observational evidence of their coincidence. This Te feature associated with the trough, known as subauroral Te increase, is due to a heat flow from the magnetosphere to the ionosphere, where the ring current particles are a major heat source. Part of this heat becomes transferred along the magnetic field lines, owing to the high thermal conductivity of the electrons, soft particle precipitations [*Kozyra et al.*, 1997; *Liemohn et al.*, 2000], and wave activity [*Gurgiolo et al.*, 2005]. This leads to an increased heat flux that gives rise to higher electron temperatures, which peak at regions of lower electron densities, like at the trough minimum and at the equatorward boundary of the polar hole, because of the greater thermal energies available per particle and less Coulomb coupling with the ions [*Moffett and Quegan*, 1983]. Many previous works such as *Brinton et al.* [1978] and *Rodger et al.* [1992], and recent statistical studies investigating the northern subauroral region such as *Kozyra et al.* [1986] and *Prolss* [2006, 2007] demonstrated that this is often the case, as subauroral Te peaks are quasi-permanent features of the plasmasphere and topside ionosphere. In order to add to these existing mainly northern hemisphere results, this study has investigated the southern latitudes and described the Ni and Te profiles utilizing field-aligned detections only. Field-aligned detections are significant, since the plasma at midlatitudes, equatorward of the trough, moves along the magnetic field lines and the subauroral Te peaks are created by field-aligned heat flows. Furthermore, this study's southern hemisphere statistical results complement the existing northern hemisphere statistical findings, and results can be compared because of the similar criteria employed. Inspecting the MLAT and Te correlations with the AE6 index, the gradients of their regression lines constructed for northern latitudes ($b_{\mathrm{MLAT}} = -0.018$ [*Prolss*, 2007]; and $b_{\mathrm{MLAT}} = -0.011$ and $b_{\mathrm{Te}} = 1.32$ [*Prolss*, 2006]) are very similar to this study's gradients of $b_{\mathrm{MLAT}} = -0.014$ and $b_{\mathrm{Te}} = 1.315$. Although those studies utilized the un-averaged Dst data, their MLAT and Te correlations with the Dst index ($b_{\mathrm{MLAT}} = 0.08$ and $b_{\mathrm{Te}} = -9.87$ [*Prolss*, 2006]; and $b_{\mathrm{MLAT}} = 0.055$ and $b_{\mathrm{Te}} = -8.03$ [*Kozyra et al.*, 1986])

Figure 7. (top) Two magnetic field lines, oriented N–S at 120°E and 312°E, and the magnetic and dip equators are indicated in the global magnetic field line map. (bottom) For these two geographic longitudes, the field-aligned latitude profiles of plasma density (Ni), electron temperature (Te), and fractional amounts of $[O^+]$, $[H^+]$, and $[He^+]$ are constructed from their respective maps shown in Figure 3.

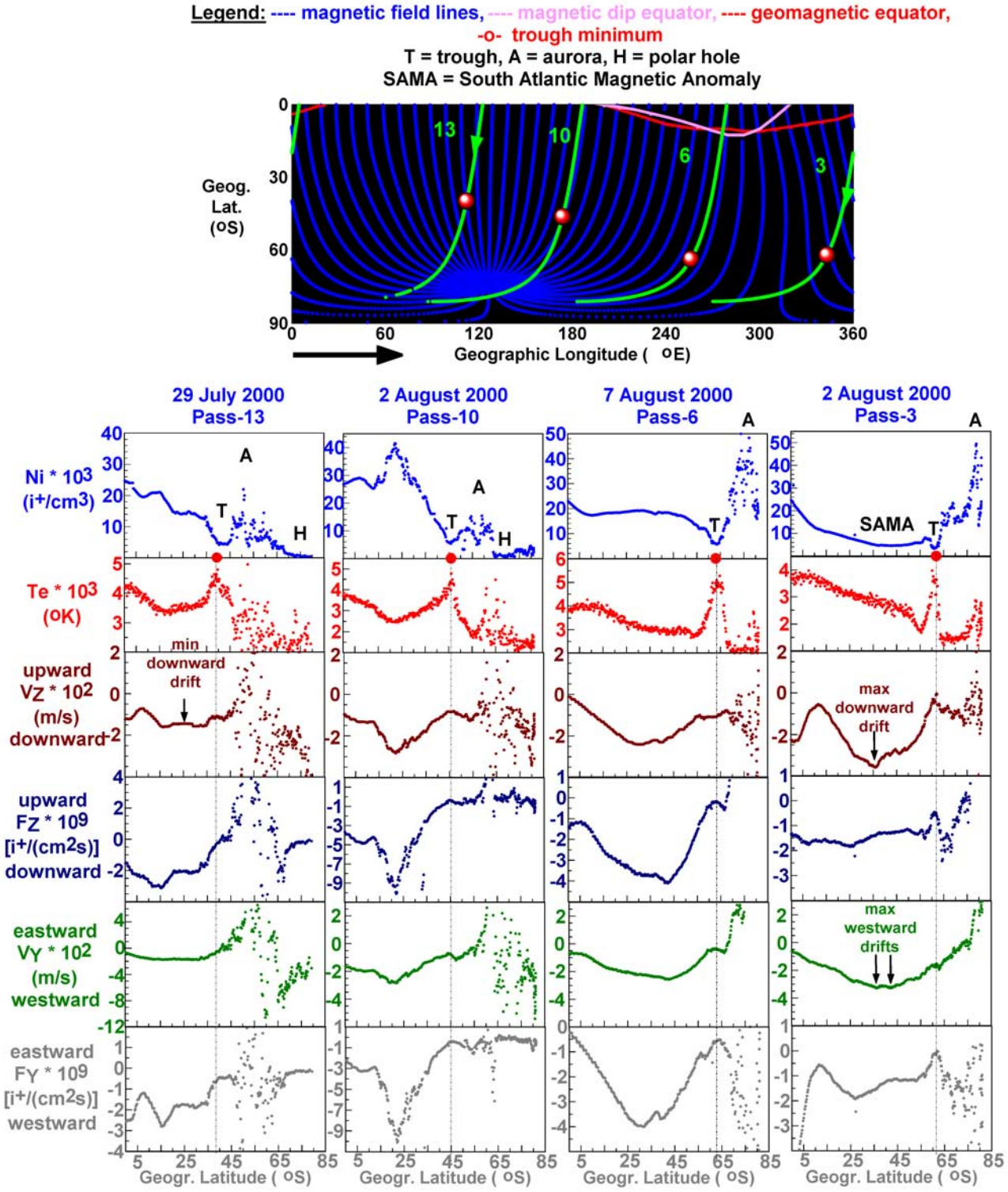

Figure 8. (top) The southern hemisphere map illustrates the ground tracks of F13 passes shown below, the magnetic field lines, the magnetic and dip equators, and the trough minima detected. (bottom) A set of four line plots illustrates the variation of plasma density (Ni), electron temperature (Te), vertical plasma drift (V_Z), vertical plasma flux (F_Z), horizontal plasma drift (V_Y), and horizontal plasma flux (F_Y) across the southern hemisphere.

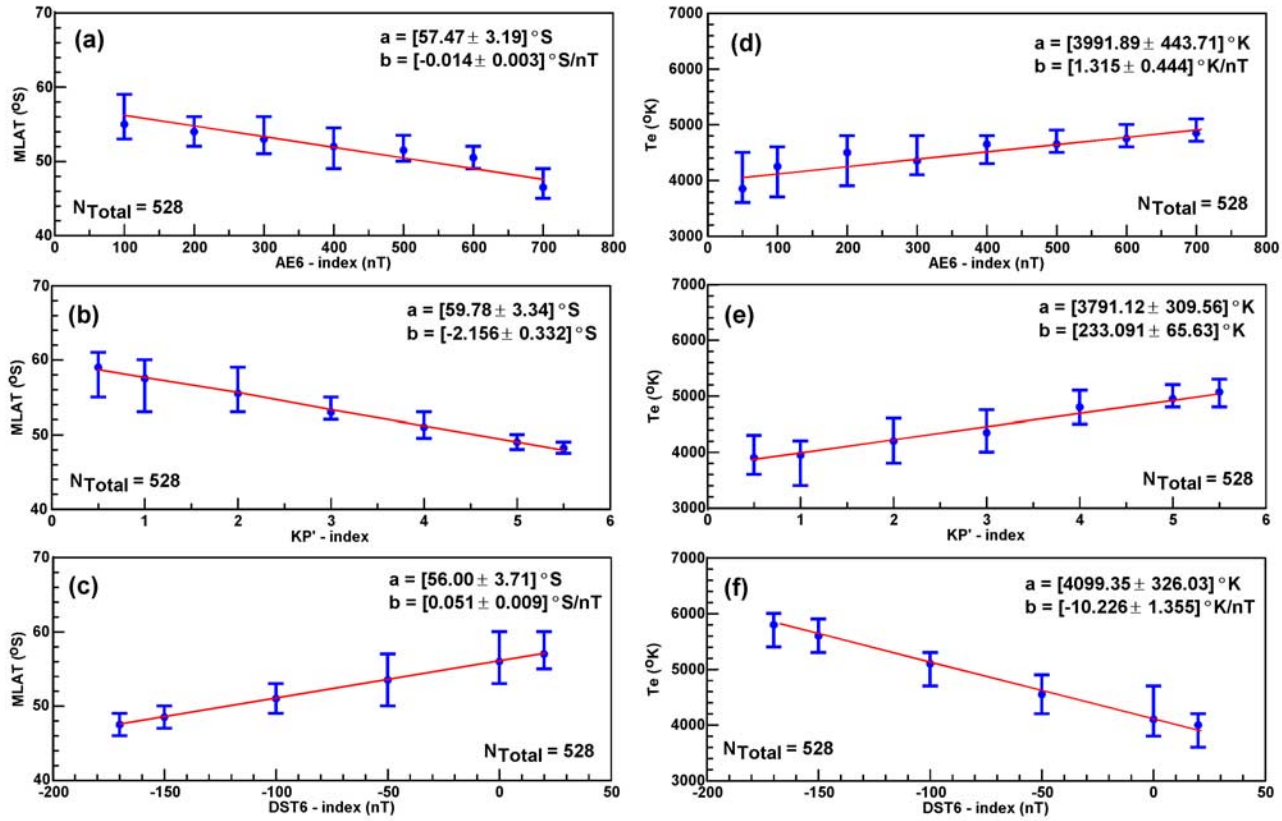

Figure 9. (a–c) The error bar plots show the statistical variation of the southern winter nighttime trough/subauroral Te peak position in magnetic latitude (MLAT) with the level of magnetic activity probed by the AE6 (Figure 9a), Kp′ (Figure 9b), and DST6 (Figure 9c) indices. (d–f) The error bar plots show the statistical variation of the subauroral Te peak magnitude (°K) with the level of magnetic activity probed by the AE6 (Figure 9d), Kp′ (Figure 9e), and DST6 (Figure 9f) indices.

are very similar to this study's DST6 correlation results of $b_{MLAT} = 0.051$ and $b_{Te} = -10.226$. Those authors found the Kp index a poor indicator of the level of magnetic activity and preferred to use the highest Kp value of the previous 12-h period known as the Kp′ index. This study adopted their technique. Their Te correlations with the Kp′ index yielded a gradient of $b_{Te} = 318.56$ [*Kozyra et al.*, 1986] that is ~75% higher than this study's gradient values of $b_{Te} = 233.091$. Regarding the *a* parameter, their AE6 correlation results show slightly different MLAT intercepts ($a_{MLAT} = 60.7$; *Prolss*, 2006 and $a_{MLAT} = 70.2$; *Prolss*, 2007) compared to this studies value of $a_{MLAT} = 57.47$. Similarly, a minor difference is shown by the Dst correlation ($a_{MLAT} = 60.7$; *Prolss*, 2007) compared to this study's result of $a_{MLAT} = 56.00$. Regarding the *a* parameters of the Te plots, there are major differences that can be explained with the different altitudes at which the data were taken. This study's Te measurements, collected at ~850 km, are substantially higher. Because of these altitude differences, the ordinate intercepts of the linear regression lines cannot be compared. However, the high (~4000°K) Te values, which were measured directly in this study during the magnetically quite times, were approximated by *Prolss* [2007] when the height variation of the subauroral Te peak was modeled. This good agreement confirms their modeling in an independent way.

5.2. Special Electrodynamic Effects Over the SAMA and Resultant Morphology

[30] At night, the rapid ion loss by recombination occurring at lower altitudes induces a downward diffusion in the topside ionosphere. Its varying intensity is controlled by the varying net effects of the equatorial vertical $\mathbf{E} \times \mathbf{B}$ drift, meridional and transequatorial neutral winds, and the SAMA's special electrodynamics [*West and Heelis*, 1996; *Abdu et al.*, 2005; *Kil et al.*, 2006]. In this study, the net effects of these components on the topside ionosphere, at around the apex height of the flux tubes, on which the interhemispheric plasma transport occurred, were investigated during southern winter when usually the interhemispheric plasma transport reaches its seasonal maximum in the Atlantic sector [*Venkatraman and Heelis*, 2000]. Evidence has been provided by the V_Z map that during the period investigated, the maximum southern (winter) downward flows were largely accelerated by the SAMA's special electrodynamic effects, as the westward conductivity gradient maximized over the South Atlantic. Furthermore, there was also an increase in the downward drift due to recombination at lower altitudes that contributed, to a lesser extent, to the acceleration of this downward flow. As a result of these, a net maximum downward drift developed over the South Atlantic. The area affected was characteristic to the SAMA's high-

conductivity region, as the SAMA's special electrodynamic effects were chiefly responsible for the creation of this maximum downward drift. This study's high-resolution V_Z map, shown in Figures 4a and 4b, tracked the net drifts ((−500 to −448) m/s)), and thus marked this high-conductivity region, and permitted to identify its alignment. Meanwhile, the V_Y map, shown in Figures 4e and 4f, tracked the region of increased net horizontal westward drifts (i.e., the horizontal component of the field-aligned (winter) downward drift), around (−500 to −436) m/s, over the same area that was registered by the V_Z map. This high V_Y region had the same magnetic alignment as that of the high V_Z region. Thus, in an independent way, these V_Z and V_Y maps have clearly defined the high-conductivity region of the SAMA for the first time, and revealed its strong magnetic alignment.

[31] This study's plasma density and composition maps (see Figure 3) detected the resulting morphology simultaneously and independently. In the SAMA region, the strongest downward drift (see also last column of Figure 8) accelerated both the heavy-ion loss (Ni $\approx 1 \bullet 10^4$ i^+/cm^3 in dark brown; $[O^+] \approx 0.04$, in dark brown, see Figures 3a and 3b and Figures 3e and 3f, respectively) by lowering the *F* region heights to altitudes of high recombination rates and the light-ion enhancement ($[H^+] > 0.9$ in red; see Figures 3g and 3h) by maximizing the plasmaspheric return flow of H^+ (see also right panel of Figure 7). Meanwhile, the maximum westward drifts moved the plasma away from the SAMA region and also contributed to the formation of low plasma densities that were registered by the Ni map over the same region that were tracked by the V_Z and V_Y maps, the SAMA's high-conductivity region.

[32] In the daytime northern hemisphere, between 20°N and 40°N (geographic), the detected net upward diffusion ($>120 \bullet 10^7$ $[i^+/(cm^2s)]$ in red; see Figures 4a–4d) was due to the interhemispheric upward (summer) flows (>70 m/s in red; see Figure 4b). The composition maps (see Figure 3) and their respective field-aligned profiles (see right panel of Figure 7) tracked the highest heavy-ion concentrations (Ni $\approx (73-82) \bullet 10^4$ i^+/cm^3; in dark purple and $[O^+] \approx 0.9$ in pink; see Figures 3a and 3b and Figures 3e and 3f, respectively) and minimum light-ion concentrations ($[H^+] \approx 0.01$ and $[He^+] \approx 0.05$ in dark brown; see Figures 3g and 3h and Figures 3i and 3j, respectively). Over the Atlantic, these northern (summer) upward plasma flows reached their seasonal maximum showing good agreement with the study of *Venkatraman and Heelis* [2000].

[33] By tracking the vertical and horizontal components of the high-latitude convection $\mathbf{E} \times \mathbf{B}$ drift, the paramount importance of plasma stagnation in the development of midlatitude trough and of the slow plasma flow in the development of polar hole have been demonstrated. Because of the weak magnetic **B** field and strong **E** field in the SAMA region, the V_Z and V_Y components were strongest at trough latitudes over the South Atlantic and created the most pronounced stagnation events (see last column in Figure 8).

6. Summary and Conclusion

[34] This study has investigated the morphology of the nighttime topside ionosphere over the southern hemisphere during the 2000 southern winter utilizing in situ multi-instrument data recorded by the DMSP-F13 spacecraft. A statistical investigation on the southern midlatitude trough and subauroral electron temperature enhancement has also been performed in order to correlate them with the level of magnetic activity probed by the AE6, Dst6 and Kp′ indices, and to model their magnetic activity dependency. A novel way to map the DMSP data spatially and in latitude provided the ability to track large-scale structures in the heavy-ion and light-ion concentrations, in electron temperatures, and in vertical and horizontal plasma drifts and flows, and to relate them.

[35] This complex investigation provided the following significant findings related to the southern midlatitude trough. In the various longitude sectors, the field-aligned trough detections revealed how the appearance of the trough varied longitudinally. Evidence has shown that these longitudinal variations were due to the longitudinal variation of the background plasma density and underlying convective plasma flows. Some field-aligned Ni-Te observations, compared with non-field-aligned ones depicting distorted cross sections, have demonstrated the significance of utilizing field-aligned detections when equatorward and poleward trough boundaries are identified, and when subauroral Te peaks are researched. On the basis of the ∼50 field-aligned detections, a Te gradient change, from shallower to steeper toward the trough minimum, was found to be a reliable signature of the trough boundary on either side of the rough minimum. Some field-aligned observations and the modeled magnetic field have also demonstrated occasions when the detected trough and plasmapause appeared on the same magnetic field line during periods of increasing magnetic activity. These examples have clearly demonstrated that the latitude difference between two trough features or between a trough feature and the plasmapause should be measured along the magnetic field line only. Statistical investigations permitted to create models that have revealed that both the trough location and the subauroral Te showed linear variations with the AE6, Dst6 and Kp′ indices. These model results show very good agreement with the relevant northern hemisphere results of *Kozyra et al.* [1986] and *Prolss* [2006, 2007].

[36] This study's investigations related to the SAMA region provided the following significant findings. The SAMA's special electrodynamic effects, induced by the weak geomagnetic **B** field, high westerly declination and high conductivity, greatly accelerated the interhemispheric southern (winter) downward plasma flows over the SAMA's high-conductivity region over the South Atlantic. The area affected by these special electrodynamic effects was tracked, for the first time, independently and simultaneously by the V_Z and V_Y plasma drift maps revealing also the strong magnetic alignment of this area. The maximum downward and westward drifts had a significant role in depleting the plasma density in the SAMA region by transporting the plasma to lower altitudes where the recombination rate was high and by moving the plasma westward, away from this region. The Ni map tracked the resultant low plasma densities over the same area (i.e., the SAMA's high-conductivity region) that was registered by the V_Z and V_Y maps. As the convective $\mathbf{E} \times \mathbf{B}$ drifts became also affected (increased) by the SAMA effects, the plasma stagnations were most pronounced over the South Atlantic. Interestingly, the southern trough appeared in its

least developed form there, in the SAMA region, because of the low background (equatorward) ionization created by the SAMA's low plasma density region.

[37] **Acknowledgments.** This research was supported by a University of Queensland Postdoctoral Research Fellowship. NICTA is funded by the Australian Government's Backing Australia's Ability initiative, in part through the Australian Research Council. The authors are thankful to the DMSP project team for the data and to M. Hairston for his advice. The AE, Dst, and Kp indices are from WDC-2 at Kyoto (http://swdcdb.kugi.kyoto-u.ac.jp).

[38] Wolfgang Baumjohann thanks Fabio Becker-Guedes and another reviewer for their assistance in evaluating this paper.

References

Abdu, M. A., and I. S. Batista (1977), Sporadic E-layer phenomena in the Brazilian magnetic anomaly: Evidence for a regular particle ionization source, *J. Atmos. Terr. Phys.*, *39*, 723–732, doi:10.1016/0021-9169(77)90059-9.

Abdu, M. A., I. S. Batista, A. J. Carrasco, and C. G. M. Brum (2005), South Atlantic magnetic anomaly ionization: A review and a new focus on electrodynamic effects in the equatorial ionosphere, *J. Atmos. Sol. Terr. Phys.*, *67*, 1643–1657, doi:10.1016/j.jastp.2005.01.014.

Abdu, M. A., J. W. MacDougall, I. S. Batista, J. H. A. Sobral, and P. T. Jayachandran (2003), Equatorial evening prereversal electric field enhancement and sporadic *E* layer disruption: A manifestation of *E* and *F* region coupling, *J. Geophys. Res.*, *108*(A6), 1254, doi:10.1029/2002JA009285.

Aladjev, G. A., O. V. Evstafiev, V. S. Mingalev, G. I. Mingalev, E. D. Tereshchenko, and B. Z. Khudukon (2001), Interpretation of ionospheric F region structures in the vicinity of ionization troughs observed by satellite radio tomography, *Ann. Geophys.*, *19*, 25–36.

Bailey, G. J., N. Balan, and Y. Z. Su (1997), The Sheffield University plasmasphere-ionosphere model: A review, *J. Atmos. Terr. Phys.*, *59*, 1541–1552, doi:10.1016/S1364-6826(96)00155-1.

Balan, N., and G. J. Bailey (1995), Equatorial plasma fountain and its effects: Possibility of an additional layer, *J. Geophys. Res.*, *100*, 21,421–21,432, doi:10.1029/95JA01555.

Balan, N., G. J. Bailey, M. A. Abdu, K. I. Oyama, P. G. Richard, J. MacDougall, and I. S. Batista (1997), Equatorial plasma fountain and its effects over three locations: Evidence for an additional layer, the F_3 layer, *J. Geophys. Res.*, *102*, 2047–2056, doi:10.1029/95JA02639.

Balan, N., I. S. Batista, M. A. Abdu, J. MacDougall, and G. J. Bailey (1998), Physical mechanism and statistics of occurrence of an additional layer in the equatorial ionosphere, *J. Geophys. Res.*, *103*, 29,169–29,181, doi:10.1029/98JA02823.

Balan, N., S. V. Thampi, K. Lynn, Y. Otsuka, H. Alleyne, S. Watanabe, M. A. Abdu, and B. G. Fejer (2008), F_3 layer during penetration electric field, *J. Geophys. Res.*, *113*, A00A07, doi:10.1029/2008JA013206.

Brinton, H. C., J. M. Grebowsky, and L. H. Brace (1978), The high-latitude winter *F* region at 300 km: Thermal plasma observations from AE-C, *J. Geophys. Res.*, *83*, 4767–4776, doi:10.1029/JA083iA10p04767.

Crowley, G., H. C. Carlson, S. Basu, W. F. Denig, J. Buchau, and B. W. Reinisch (1993), The dynamic ionospheric polar hole, *Radio Sci.*, *28*, 401–413, doi:10.1029/92RS02878.

Fejer, B. G., J. W. Jensen, and S.-Y. Su (2008), Quiet time equatorial *F* region vertical plasma drift model derived from ROCSAT-1 observations, *J. Geophys. Res.*, *113*, A05304, doi:10.1029/2007JA012801.

Fok, M.-C., J. U. Kozyra, and L. H. Brace (1991), Solar cycle variation in the subauroral electron temperature enhancement: Comparison of AE-C and DE 2 satellite observations, *J. Geophys. Res.*, *96*, 1861–1866, doi:10.1029/90JA02377.

Gurgiolo, C., B. R. Sandel, J. D. Perez, D. G. Mitchell, C. J. Pollock, and B. A. Larsen (2005), Overlap of the plasmasphere and ring current: Relation to subauroral heating, *J. Geophys. Res.*, *110*, A12217, doi:10.1029/2004JA010986.

Hairston, M. R., R. Heelis, and F. Rich (1997), Analysis of the ionospheric cross polar cap potential drop and polar ion convection patterns during the January 1997 CME events using DMSP data, *Eos Trans. AGU*, *78*, 264.

Hanson, W. B., and R. J. Moffett (1966), Ionization transport effects in the equatorial *F* region, *J. Geophys. Res.*, *71*, 5559–5572.

Heelis, R. A. (1984), The effects of the interplanetary magnetic field orientation on dayside high-latitude ionospheric convection, *J. Geophys. Res.*, *89*, 2873–2880, doi:10.1029/JA089iA05p02873.

Heelis, R. A., J. A. Murphy, and W. B. Hanson (1981), A feature of the behavior of He^+ in the nightside high-latitude ionosphere during equinox, *J. Geophys. Res.*, *86*, 59–64, doi:10.1029/JA086iA01p00059.

Horvath, I. (2007), Impact of 10 January 1997 geomagnetic storm on the nighttime Weddell Sea Anomaly: A study utilizing data provided by the TOPEX/Poseidon mission and the Defense Meteorological Satellite Program, and simulations generated by the Coupled Thermosphere/Ionosphere Plasmasphere model, *J. Geophys. Res.*, *112*, A06329, doi:10.1029/2006JA012153.

Horwitz, J. L., R. H. Comfort, P. G. Richards, M. O. Chandler, C. R. Chappell, P. Anderson, W. B. Hanson, and I. H. Brace (1990), Plasmasphere-ionosphere coupling, 2. Ion composition measurements at plasmaspheric and ionospheric altitudes and comparison with modeling results, *J. Geophys. Res.*, *95*, 7949–7959, doi:10.1029/JA095iA06p07949.

Karpachev, A. T. (2003), The dependence of the main ionospheric trough shape on longitude, altitude and season, local time and solar and magnetic activity, *Geomagn. Aeron.*, *32*, 665–668.

Kendall, P. C., and W. M. Pickering (1967), Magnetoplasma diffusion at F2-region altitudes, *Planet. Space Sci.*, *15*, 825–833, doi:10.1016/0032-0633(67)90118-3.

Kil, H., R. DeMajistre, L. J. Paxton, and Y. Zhang (2006), Nighttime *F* region morphology in the low and middle latitudes seen from DMSP F15 and TIMED/GUVI, *J. Atmos. Sol. Terr. Phys.*, *68*, 1672–1681, doi:10.1016/j.jastp.2006.05.024.

Knudsen, W. C. (1974), Magnetospheric convection and the high-latitude F_2 ionosphere, *J. Geophys. Res.*, *79*, 1046–1055, doi:10.1029/JA079i007p01046.

Kozyra, J. U., L. H. Brace, T. E. Cravens, and A. F. Nagy (1986), A statistical study of the subauroral electron temperature enhancement using Explore 2 Langmuir probe observations, *J. Geophys. Res.*, *91*, 11,270–11,280, doi:10.1029/JA091iA10p11270.

Kozyra, J. U., A. F. Nagy, and D. W. Slater (1997), High-altitude energy source(s) for stable auroral red arcs, *Rev. Geophys.*, *35*, 155–190, doi:10.1029/96RG03194.

Kutiev, I., R. A. Heelis, and S. Sanatani (1980), The behavior of the O^+-H^+ transition level at solar maximum, *J. Geophys. Res.*, *85*, 2366–2372, doi:10.1029/JA085iA05p02366.

Liemohn, M. W., J. U. Kozyra, P. G. Richards, G. V. Khazanov, M. J. Buonsanto, and V. K. Jordanova (2000), Ring current heating of the thermal electrons at solar maximum, *J. Geophys. Res.*, *105*, 27,767–27,776, doi:10.1029/2000JA000088.

Moffett, R. J., and S. Quegan (1983), The mid-latitude trough in the electron concentration of the ionospheric F-layer: A review of observations and modeling, *J. Atmos. Terr. Phys.*, *45*, 315–343, doi:10.1016/S0021 9169(83)80038-5.

Muldrew, D. B. (1965), *F*-layer ionization trough deduced from Alouette data, *J. Geophys. Res.*, *70*, 2635–2650, doi:10.1029/JZ070i011p02635.

Newell, P. T., Y. I. Feldstein, Y. I. Galperin, and C.-I. Meng (1996), Morphology of nightside precipitation, *J. Geophys. Res.*, *101*, 10,737–10,748, doi:10.1029/95JA03516.

Prolss, G. W. (2006), Subauroral electron temperature enhancement in the nighttime ionosphere, *Ann. Geophys.*, *24*, 1871–1885.

Prolss, G. W. (2007), The equatorial wall of the subauroral trough in the afternoon/evening sector, *Ann. Geophys.*, *25*, 645–659.

Rodger, A. S. (1984), Spread-F ionospheric irregularities and their relationship to stable auroral red arcs at magnetic mid-latitudes, *J. Atmos. Terr. Phys.*, *46*, 335–342, doi:10.1016/0021-9169(84)90117-X.

Rodger, A. S., and J. Aarons (1988), Studies of ionospheric *F* region irregularities from geomagnetic mid-latitude conjugate regions, *J. Atmos. Terr. Phys.*, *50*, 63–72, doi:10.1016/0021-9169(88)90010-4.

Rodger, A. S., R. J. Moffett, and S. Quegan (1992), The role of ion drift in the formation of ionization troughs in the mid- and high-latitude ionosphere—A review, *J. Atmos. Terr. Phys.*, *54*, 1–30, doi:10.1016/0021-9169(92)90082-V.

Sharp, G. W. (1966), Mid-latitude trough in the night ionosphere, *J. Geophys. Res.*, *71*, 1345–1356.

Sojka, J. J., R. W. Schunk, W. R. Hoegy, and J. M. Grebowsky (1991), Model and observation comparison of the universal time and IMF BY dependence of the ionospheric polar hole, *Adv. Space Res.*, *11*(10), 39–42.

Titheridge, J. E. (1995), Winds in the ionosphere—A review, *J. Atmos. Terr. Phys.*, *57*, 1681–1714, doi:10.1016/0021-9169(95)00091-F.

Trivedi, N. B., B. M. Pathan, N. J. Schuch, M. Barreto, and L. G. Dutra (2005), Geomagnetic phenomena in the South Atlantic anomaly region in Brazil, *Adv. Space Res.*, *36*, 2021–2024, doi:10.1016/j.asr.2004.09.020.

Venkatraman, S., and R. Heelis (1999), Longitudinal and seasonal variations in nighttime plasma temperatures in the equatorial topside ionosphere during solar maximum, *J. Geophys. Res.*, *104*(A2), 2603–2611.

Venkatraman, S., and R. Heelis (2000), Interhemispheric plasma flows in the equatorial topside ionosphere, *J. Geophys. Res.*, *105*, 18,457–18,464, doi:10.1029/2000JA000012.

Voiculescu, M., I. Virtanen, and T. Nygren (2006), The *F* region trough: Seasonal morphology and relation to interplanetary magnetic field, *Ann. Geophys.*, *24*, 173–185.

Werner, S., and G. W. Prolss (1997), The position of the ionospheric trough as a function of local time and magnetic activity, *Adv. Space Res.*, *20*(9), 1717–1722, doi:10.1016/S0273-1177(97)00578-4.

West, K. H., and R. A. Heelis (1996), Longitude variations in ion composition in the morning and evening topside equatorial ionosphere near solar minimum, *J. Geophys. Res.*, *101*, 7951–7960, doi:10.1029/95JA03377.

Whalen, J. A. (1989), The daytime *F* layer trough and its relation to ionospheric-magnetospheric convection, *J. Geophys. Res.*, *94*, 17,169–17,184, doi:10.1029/JA094iA12p17169.

Yizengaw, E., and M. B. Moldwin (2005), The altitude extension of the mid-latitude trough and its correlation with plasmapause position, *Geophys. Res. Lett.*, *32*, L09105, doi:10.1029/2005GL022854.

Yizengaw, E., H. Wei, M. B. Moldwin, D. Galvan, L. Mandrake, A. Manucci, and X. Pi (2005), The correlation between the mid-latitude trough and the plasmapause, *Geophys. Res. Lett.*, *32*, L10102, doi:10.1029/2005GL022954.

I. Horvath and B. C. Lovell, SAS, School of Information Technology and Electrical Engineering, University of Queensland, Brisbane, Qld 4072, Australia. (ihorvath@itee.uq.edu.au)